Cell Reports

Article

Delamination of trophoblast-like syncytia from the amniotic ectodermal analogue in human primed embryonic stem cell-based differentiation model

Graphical abstract

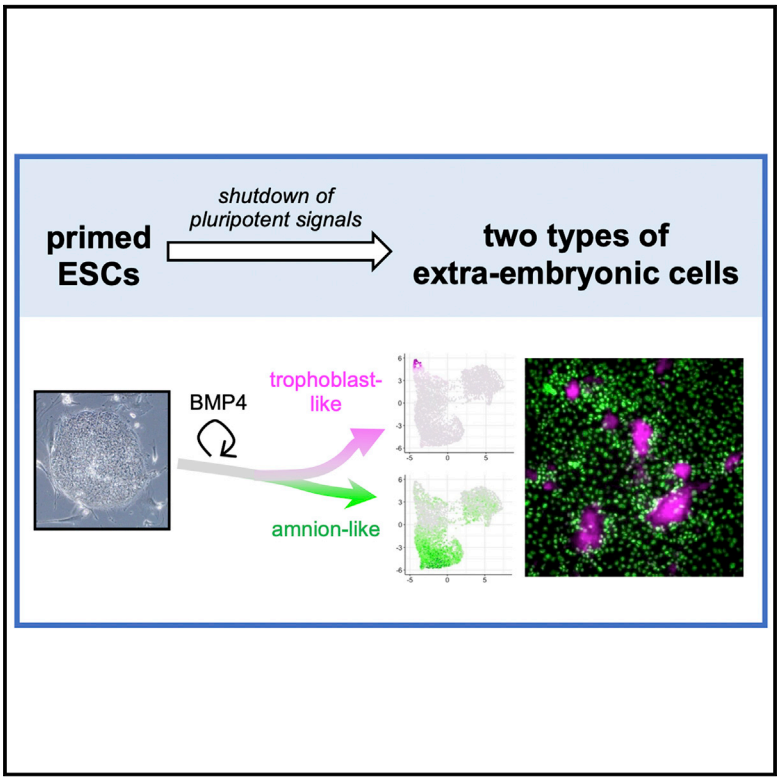

Authors

Masatoshi Ohgushi, Nobuko Taniyama, Alexis Vandenbon, Mototsugu Eiraku

Correspondence

mohgushi@infront.kyoto-u.ac.jp

In brief

Ohgushi et al. show that chemical blockade of ACTIVIN/NODAL and FGF signals activates BMP signaling and steers human primed ESCs into GATA3-expressing cells that consist of two types of cells, one showing an STB-like phenotype and the other resembling amnion ectoderm. These results suggest a possible primate-specific extraembryonic differentiation pathway.

Highlights

- Blocking pluripotent signals converts human primed ESCs into GATA3^{+} cells
- Cell-autonomous BMP signals are crucial for the extraembryonic fate decision
- The differentiating cells are bifurcated into two types of extraembryonic lineages

Ohgushi et al., 2022, Cell Reports *39*, 110973
June 21, 2022
https://doi.org/10.1016/j.celrep.2022.110973

CellPress

Cell Reports

CellPress
OPEN ACCESS

Article

Delamination of trophoblast-like syncytia from the amniotic ectodermal analogue in human primed embryonic stem cell-based differentiation model

Masatoshi Ohgushi,[1,2,5,*] Nobuko Taniyama,[1] Alexis Vandenbon,[4] and Mototsugu Eiraku[1,2,3]

[1]Laboratory of Developmental Systems, Institute for Life and Medical Sciences, Kyoto University, Shogoin Kawahara-cho, Sakyo-ku, Kyoto 606-8507, Japan

[2]Laboratory of Organoids Technology, Center for Human ES Cell Research, Institute for Life and Medical Sciences, Kyoto University, Shogoin Kawahara-cho, Sakyo-ku, Kyoto 606-8507, Japan

[3]Institute for Advanced Study of Human Biology (WPI-ASHBi), Kyoto University, Yoshida-Konoe-cho, Sakyo-ku, Kyoto 606-8501, Japan

[4]Laboratory of Tissue Homeostasis, Institute for Life and Medical Sciences, Kyoto University, Shogoin Kawahara-cho, Sakyo-ku, Kyoto 606-8507, Japan

[5]Lead contact

*Correspondence: mohgushi@infront.kyoto-u.ac.jp

https://doi.org/10.1016/j.celrep.2022.110973

SUMMARY

Human primed embryonic stem cells (ESCs) are known to be converted to cells with several trophoblast properties, but it has remained controversial whether this phenomenon represents the inherent differentiation competence of human primed ESCs to trophoblast lineages. In this study, we report that chemical blockage of ACTIVIN/NODAL and FGF signals is sufficient to steer human primed ESCs into GATA3-expressing cells that give rise to placental hormone-producing syncytia analogous to syncytiotrophoblasts of the post-implantation stage of the human embryo. Despite their cytological similarity to syncytiotrophoblasts, these syncytia arise from the non-trophoblastic differentiation trajectory that recapitulates amniogenesis. These results provide insights into the possible extraembryonic differentiation pathway that is unique in primate embryogenesis.

INTRODUCTION

In mammalian development, a totipotent fertilized egg undergoes a series of cell divisions while differentiating into several lineages in a stepwise manner. Genetic studies using mice as model animals have established the concept that the first cell fate specification in mammals, the inner cell mass (ICM) or trophectoderm (TE) lineage specification, starts around the morula stage, and then they are segregated to form a blastocyst. TE provides multiple components of the placenta that play important roles in implantation and fetal growth. ICM is a transient pluripotent tissue that segregates into two lineages, primitive endoderm and epiblast (reviewed in Rossant, 2018). According to the correspondence to these developmental stages, pluripotency is classified into several types. In particular, the preimplantation ICM/epiblast is regarded as naive, whereas post-implantation epiblast represents primed state of pluripotency (Nichols and Smith, 2009). Mouse embryonic stem cells (mESCs), a cell line derived from ICMs, recapitulate the naive pluripotency of the parental tissue. When injected into blastocysts, mESCs are incorporated into the ICM tissue and start to differentiate following the developmental program of the host animals. In chimeric pups, mESC derivatives are distributed in multiple tissues, except for the placenta. This provides strong evidence that mESCs possess pluripotency but lack the competence to differentiate into trophoblast lineages. Indeed, trophoblast differentiation from mESCs is not attainable *in vitro* unless artificial genetic manipulations are conducted, while they can differentiate into cells of all three germ layers (Martello and Smith, 2014). The inability to differentiate into trophoblast lineages is also applicable to the stem cells derived from mouse post-implantation epiblast, EpiSCs, which are in the primed state of pluripotency.

The consensus that pluripotent stem cells never differentiate into trophoblast lineages has been challenged by a surprising report showing that human ESCs, which are now considered to be corresponding to mouse EpiSCs, were converted into differentiated cells with unique properties for placental cells just by exposing them to BMP4 (Xu et al., 2002; the human conventional ESCs are now referred as primed ESCs). Many groups succeeded in replicating this phenomenon; in particular, the establishment of a protocol to achieve the efficient conversion of human primed ESCs into trophoblasts, called a BAP (BMP4 plus ACTIVIN/NODAL blocker A83-01 and basic fibroblast growth factor (bFGF) blocker PD173074) facilitated the reproducibility (Amita et al., 2013; Roberts et al., 2018). The primed ESC-derived trophoblast-like cells have been utilized as an experimental platform for molecular and pathological studies of viral infection or placental disorders, and provide valuable information (Sheridan et al., 2017, 2019; Horii et al., 2021). It has

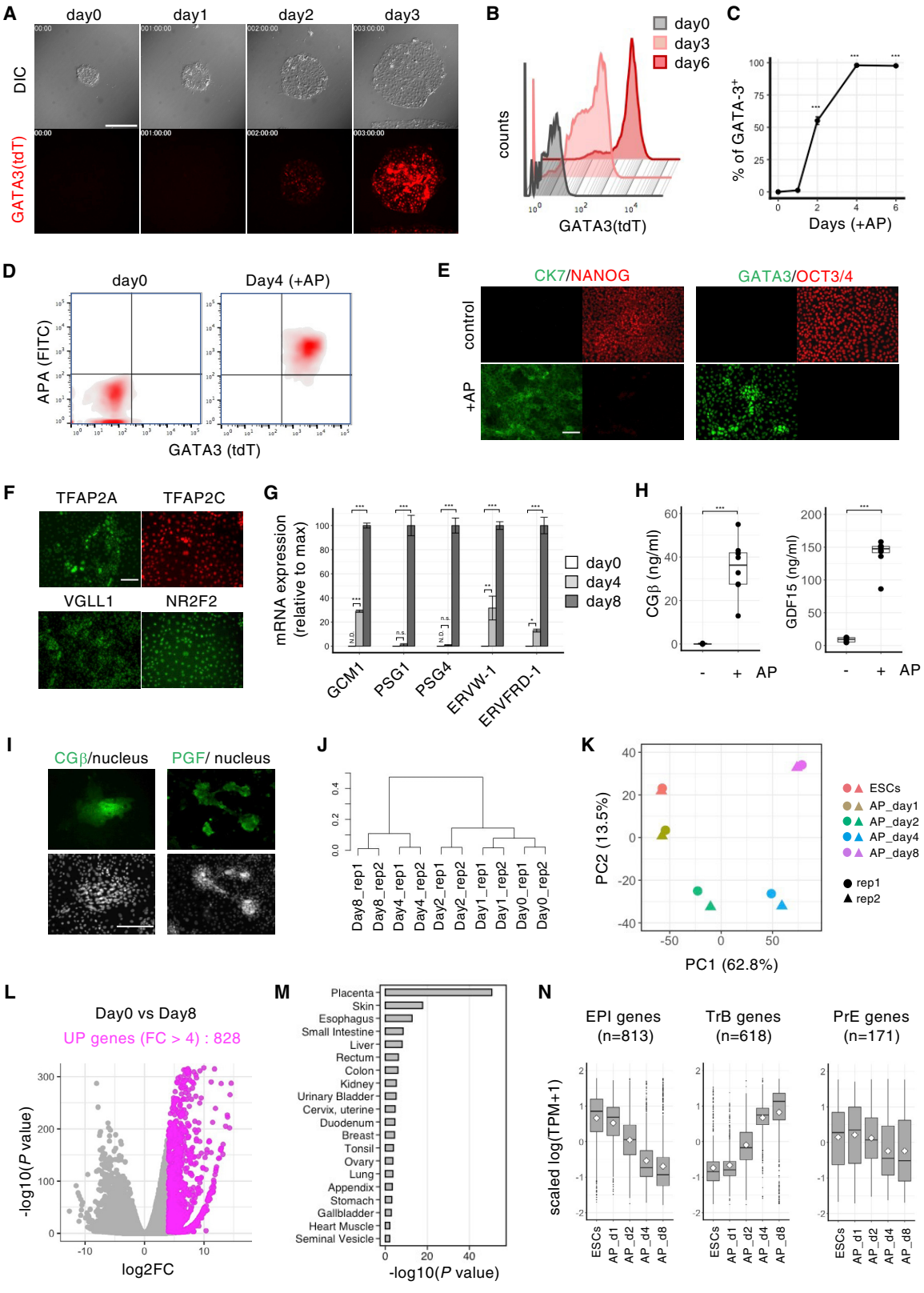

(legend on next page)

been also reported that primate primed ESCs could contribute to the extraembryonic tissues, including placenta, when injected into the monkey morula or blastocysts (Huang et al., 2018; Kang et al., 2018). Nevertheless, the reliability of the trophoblast differentiation from primed (or conventional) ESCs has been under intense debate over the past decades (Bernardo et al., 2011; Roberts et al., 2014), possibly because it contradicted the developmental dogma that has been validated in mouse studies. Recently, two groups reported that BMPs induce amnion rather than trophoblast differentiation in human primed ESCs, questioning their trophoblast competence (Guo et al., 2021; Io et al., 2021). It remains an open question whether trophoblast-like differentiation from primed ESCs recapitulates any developmental processes.

During the investigation of BAP-induced responses, we noticed that, without exogenous supplementation of BMP ligands, conventional human ESCs could be differentiated into cells expressing several extraembryonic marker genes, including GATA3. Using this differentiation system, we deciphered the cellular properties of the ESC-derived GATA3$^+$ cells and uncovered the dynamic transition from the primed pluripotent cells to two types of extraembryonic cells; amnionic ectoderm-like cells and syncytiotrophoblast-like syncytial cells.

RESULTS

ACTIVIN/FGF blockers alone are sufficient to generate GATA3$^+$ cells from human primed ESCs

To investigate the dynamic process of trophoblast-like differentiation from human ESCs, we generated reporter cell lines by applying GATA3 as a readout for the trophoblast identity (G3KI cells, clones #2–5- and #30–1; Figures S1A and S1B). We confirmed that these reporter lines became positive for tandem tomato (tdT) upon a BAP treatment (Figure S1C).

Interestingly, during the validation of these reporter lines, we noticed that exogenous BMP4 was not essential for producing GATA3-expressing cells (Figure 1A; Video S1). Flow cytometric analyses showed that >95% of cells expressed tdT at day 4 just by adding only the two inhibitors for the ACTIVIN/NODAL and FGF signaling (Figures 1B, 1C, and S1D). These tdT$^+$ cells also expressed a panel of trophoblast-associated markers (Figures 1D–1F). Quantitative RT-PCR analyses confirmed that genes associated with placental functions, including hormone biosynthesis, nutrient transport, and immunological tolerance, showed a significant increase in their mRNA expression (Figures 1G and S1E). As different placental features, the upregulation of endogenous retroviruses and the expression and/or secretion of placental hormones chorionic gonadotrophin β (CGβ), GDF15, and PGF, were detected after cells were treated with the two inhibitors (Figures 1G–1I). These observations indicate that the combined inhibition of ACTIVIN/NODAL and FGF signals steered ESCs to express biological features unique to the placenta. We observed GATA3 induction in all culture media and substrates we tested and in other primed ESC or iPSC lines (Figures S1F–S1I). Hereafter, we denote this differentiation recipe consisting of small molecules only as an AP (BAP minus BMP4), and GATA3-expressing cells as GATA3$^+$ extraembryonic (ExE) cells to distinguish them from trophectoderm-derived conventional trophoblast lineages.

Validating cells using a small number of classical placental markers only may be a cause of controversy. Therefore, we explored the genome-wide transcriptome features and dynamics of AP-induced differentiation processes by bulk RNA sequencing. Principal component and clustering analyses indicated a drastic change in gene expression patterns between 2 and 4 days after AP addition (Figures 1J and 1K). These differentiated cells lacked the expression of markers for definitive endoderm, mesoderm, and neural progenitors (Figure S1J; Cliff et al., 2017). Then we extracted differentially expressed genes (DEGs) between ESCs and GATA3$^+$ ExE cells (at day 8) and performed gene enrichment analyses (Figure 1L). These analyses indicated that the upregulated genes were more closely associated with the placenta than other tissues and with placenta-related terms or biological processes (Figures 1M and S1K). We then examined the expression of hundreds of gene that had been reported as DEGs among three major

Figure 1. ACTIVIN/FGF blockers alone are sufficient to generate GATA3$^+$ cells from human primed ESCs

(A) Live imaging of the GATA3-knockin KhES-1 cells treated with AP for 72 h. Red fluorescence indicates GATA3-expressing cells. Recording was started immediately after AP addition. Scale bar, 500 μm.

(B and C) Time course quantitation of GATA3$^+$ cells after AP addition. (B) Representative histograms are shown. (C) Data represent the mean with SD (n = 3).

(D) Flow cytometric panels for APA$^+$/GATA3$^+$ cells at day 4 after AP addition. As a negative control, cells were incubated without a primary antibody and then stained using a fluorescein isothiocyanate (FITC)-conjugated mouse IgG antibody. The representative panels from three independent experiments are shown.

(E and F) Immunostaining for ESCs or trophoblast markers. Cells were stained before and 3 days (E), and at 4 days after AP addition (F). The representative panels from three independent experiments are shown. Scale bar, 200 μm.

(G) qPCR assay for trophoblast-related genes. GATA3-knockin KhES-1 cells were treated with AP for the indicated periods. Data represent the mean with SD (n = 3).

(H and I) Production of placental hormones. (H) Secretion level of CGβ and GDF15 in AP-treated cells (at day 8). Data represent the mean with SD (n = 8). (I) Immunostaining for CGβ and PGF at 6 days after AP addition. Representative images from three independent experiments are shown.

(J) Unbiased hierarchical clustering of the transcriptome data. GATA3-knockin KhES-1 cells were treated with AP for 0, 1, 2, 4 and 8 days with two biological replicates.

(K) Principal component analyses (PCAs) of AP-induced differentiated cells at days 0, 1, 2, 4, and 8. The top 1,000 valuable genes were used for the variation calculation.

(L and M) Volcano plot of ESCs versus differentiated cells (day 8) (L). The upregulated genes (828 genes, $\log_2$ fold change [FC] > 4, $p > 0.05$) are indicated as red dots. Tissue distribution of the upregulated genes is shown (M).

(N) Boxplot presentation showing the expression dynamics of the genes shown to be enriched in the epiblast (EPI genes; 813), trophoblast (TrB genes; 618), and primitive endoderm (PrE genes; 171) of the cultured blastocysts (Xiang et al., 2020). Statistical analyses were done by Dunnett's test (D and G) and Wilcoxon signed-rank test for paired data (H); N.D., not detected; n.s., not significant; *$p < 0.05$, **$p < 0.01$, ***$p < 0.001$. See also Figure S1 and Video S1.

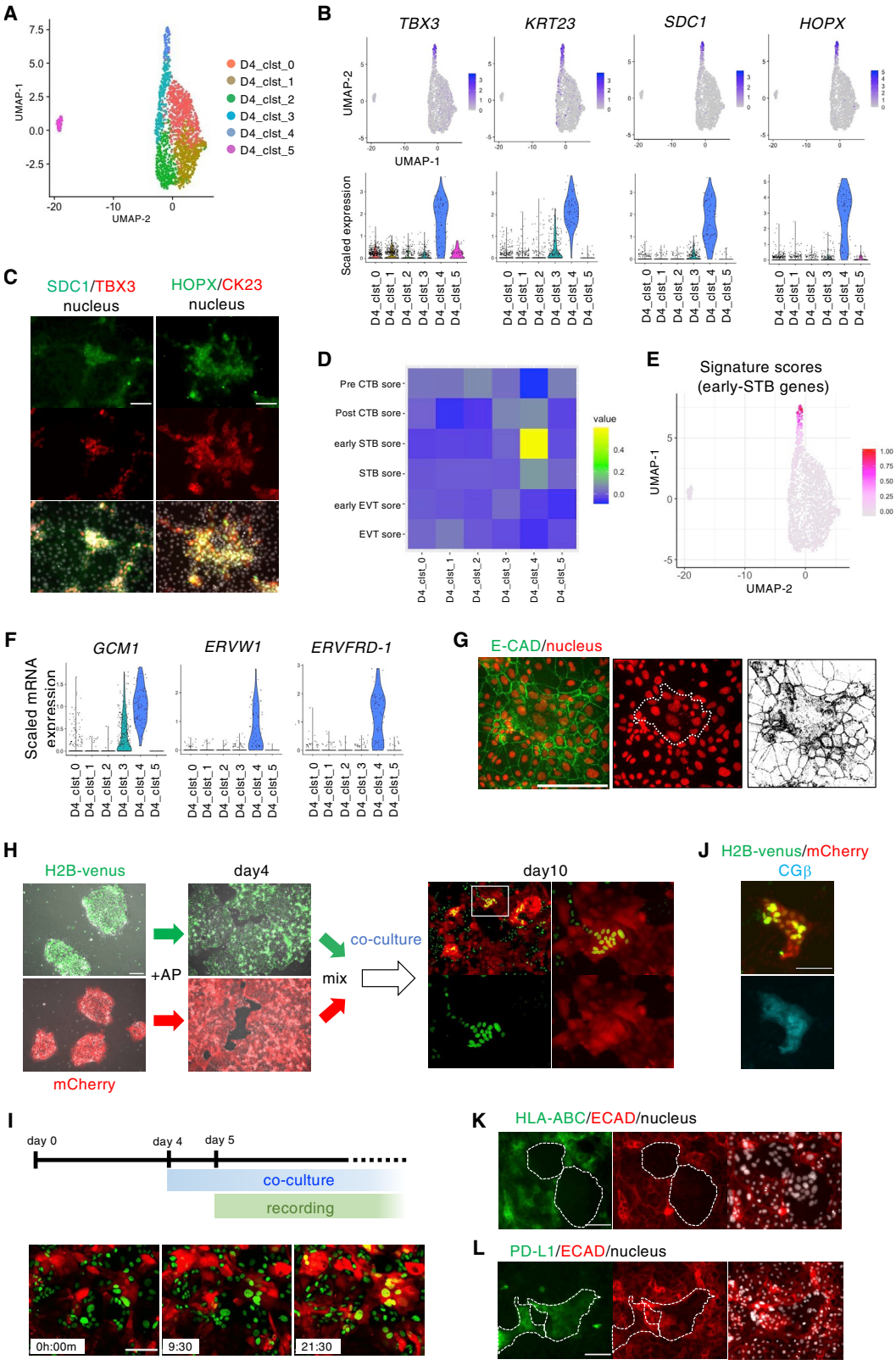

(legend on next page)

lineages residing within days post fertilization (DPF) 7–9 cultured human embryos: epiblast (EPI), primitive endoderm (PrE), and trophoblast (TrB) (Xiang et al., 2020). The temporal expression of these genes indicated an obvious trend of TrB gene induction in parallel with EPI gene downregulation (Figure 1N). These results indicated that AP alone could convert primed ESCs into cells that are assigned to the trophoblast or placenta at a global transcriptome level.

Syncytiotrophoblast-like features of AP-induced GATA3$^+$ cells

In the implantation stage of the human embryo, three types of trophoblast lineages, cytotrophoblast (CTB), syncytiotrophoblast (STB), and extravillous trophoblast (EVT), form the primitive syncytium (Turco and Moffett, 2019). For a more detailed characterization of the AP-induced GATA3$^+$ cells, the gene expression in the cells treated with AP for 4 days, the time point when almost all cells became positive for GATA3, was profiled by single-cell RNA sequencing (scRNA-seq, 10x Genomics). Clustering analyses showed that a total of 1,833 cells were divided into six clusters (Figures 2A and S2A). Profiling DEGs among these six clusters revealed that cluster 4 cells shared highly expressing genes with cells annotated as early STBs (E-STBs) and STBs of the human embryos cultured to the post-implantation stage (Xiang et al., 2020) (Figures 2B and S2B). They included several classical markers for STBs (CGβ, SDC1, and TBX3; Okae et al., 2018; Lv et al., 2019), and their expression was confirmed at a protein level (Figure 2C). As a comprehensive approach, we calculated the signature scores of each cluster using the reported DEGs among the trophoblast subpopulations of 6–14 DPF human embryos (Xiang et al., 2020), and found that cluster 4 showed a higher E-STB score than the other clusters (Figures 2D, 2E, and S2C). Due to technical limitations, a part of enlarged STB-like cells was filtered out during the processes for single-cell isolation (see STAR Methods), which might be a cause for the seemingly small proportion of cluster 4 in the single-cell analyses (77 out of 1,833 cells, 4.2%); however, live-cell immunostaining indicated that the large area of the AP-treated cells was positive for SDC1 (Figure S2D). Reanalyses of the bulk RNA-sequencing data using these DEGs indicated that the expression of E-STB- and STB-enriched genes increased with the extension of the culture period (Figure S2E).

STBs play pivotal roles in pregnancy, including hormone production, nutrient/waste exchange, and immune tolerance. They differentiated from the progenitor CTBs and formed characteristic multinucleated syncytia. Consistent with the high levels of expression of several genes implicated in cell fusion, syncytia were observed in the culture of GATA3+ ExE cells (Figures 2F and 2G). To monitor syncytium formation, two lines of ESC that were marked with different fluorescent proteins (H2B-Venus and mCherry, respectively) were independently treated with AP for 4 days, and then mixed and cocultured. After 4–6 days of coculture, we detected the appearance of syncytia, defined as cells expressing both the Venus signals in the nucleus and mCherry signals in the cell body (Figures 2H, 2I, and S2F; Video S2). We confirmed the expression of CGβ in these multinucleated syncytia (Figure 2J). These syncytia exhibited striking immunological hallmarks; they expressed immuno-suppressive programmed death-ligand 1 (PD-L1) while expressing a negligible level of class I HLA molecules (Figures 2K, 2L, S2G, and S2H). The expression of HLA-G, a typical marker for EVT, was detected, but the global trend of EVT-enriched gene expression did not support a robust EVT induction (Figures S2I and S2J).

From these results, we reasoned that, under our culture conditions, human primed ESCs differentiate into cells that were akin to STBs, rather than EVTs, of the peri-implantation embryos.

Molecular analyses of primed ESC-to-GATA3$^+$ ExE conversion

It is interesting that inhibitor-mediated perturbation of pluripotent signals was sufficient to stimulate ESCs not only to exit from their undifferentiated state but also to undergo a sequential transition into GATA3$^+$ cells. This suggests uncharacterized intrinsic programs for extraembryonic fate conversion of human primed ESCs. We sought to decipher the intrinsic mode of the differentiation program. In the scheduled medium-switching experiments, it was demonstrated that the first 3 days of inhibitor administration were sufficient to produce GATA3-positive cells with >90% efficiency (Figure S3A), indicating that this is a critical period for the fate determination of GATA3$^+$ ExE cells. We examined BMP responses during this period, because the importance of BMP

Figure 2. Syncytiotrophoblast-like features of AP-induced GATA3$^+$ cells

(A) UMAP representation of 1,833 AP-induced GATA3$^+$ cells (day 4). The six clusters can be visualized based on the colors indicated.

(B) Scatter and violin plot representations for cluster distribution of the representative genes identified as cluster 4-enriched DEGs.

(C) Immunostaining of KhES-1 cells for the indicated genes at day 5 after AP addition. Representatives from three independent experiments are shown. Scale bar, 100 μm.

(D and E) Signature scores calculated using genes specific for each trophoblast sublineage in cultured human embryos (Xiang et al., 2020). (D) Heatmap representation for signature score of each cluster. (E) Distribution of signature score calculated genes specific in early STBs (n = 218) (Xiang et al., 2020) was presented in a UMAP space.

(F) Violin plot representations for cluster distribution of the representative genes implicated in cell fusion.

(G) Confocal images of syncytia at 4 days after AP addition. A binary image of E-cadherin (ECAD) signal (right, gray image). Syncytia is defined by ECAD signal, and indicated as the enclosed regions in the right fluorescence image (dotted lines). Representative images are shown. Scale bar, 100 μm.

(H and I) Visualization of syncytium formation. Coculture was started at 4 days after differentiation. (H) Syncytia were double positive for H2B-Venus and mCherry. Fluorescent images at day 10. (I) Time-lapse confocal images of syncytialization. Scale bar, 100 μm.

(J) Immunostaining for CGβ in a H2B-Venus$^+$/mCherry$^+$ syncytium. Scale bar, 100 μm.

(K) The expression of immunomodulators in KhES-1 cells treated with AP. Cells were treated with AP for 8 days and stained with antibodies for the indicated proteins. Syncytia were defined with ECAD signal, and indicated as the enclosed regions (dotted lines).

(L) PD-L1-positive areas are indicated as enclosed regions (dotted lines). Scale bars, 200 μm. See also Figure S2 and Video S2.

signaling to direct conventional ESCs to trophoblasts has been repeatedly reported in the past decades (Roberts et al., 2018; Xu et al., 2002). Through a series of biochemical assays, we found that BMP-SMAD signaling was transiently activated by AP stimulation (Figures 3A, 3B, 3C, and 3D). When surveying bulk RNA-sequencing data, we noticed that, among BMP ligands, the mRNA expression of BMP4 was upregulated (Figures 3C and S3B). The secretion of BMP4 into the culture medium was confirmed (Figure 3D). To validate the involvement of the cell-autonomous BMP signals in the cell fate determination, we tested two different types of BMP signal blockers, NOGGIN (NOG) as an antagonist for extracellular BMPs and LDN-193189 (LDN) as a kinase inhibitor for intracellular signal cascade. These blockers impaired the upregulation of BMP reporter activity in AP-treated cells, ensuring the cell-autonomous activation of BMP signaling in the differentiating cells (Figure 3E). When BMP signal input was repressed by the combined action of NOG and LDN, the AP-induced GATA3-expressing cells were significantly decreased (Figures 3F, 3G, S3C, and S3D). Alternatively, PAX6$^+$ neuronal ectodermal cells were induced under these conditions (Figure 3G). Consistent with these results, quantitative RT-PCR analyses showed a reduction in trophoblast genes and the upregulation of ectoderm genes in the BMP-inhibited condition (Figure S3E). Simultaneous treatment of primed ESCs with AP and BMP4 (BAP) induced a rapid induction of GATA3-expressing cells, but their expression levels at the later phase were comparable with that of AP-treated cells (Figure S3F).

Taken together, these results demonstrated that cell-autonomous BMP signal activation is important for the efficient conversion of primed ESCs into the extraembryonic fate. We inferred that, upon exit from an undifferentiated state, cells begin to express and secret BMP4, and this endogenous signal determines the fate into the GATA3$^+$ ExE cells while preventing ectodermal fate.

Amniotic features at the early phase of differentiation

The BMP4-expressing cells are key for determining the fate of GATA3$^+$ ExE cells. We supposed that these cells are analogous to the amniotic ectoderm, the EPI-derived epithelium that underlies the trophoblast layer to form an amniotic cavity in peri-implantation primate embryos, since *BMP4* mRNA was detected in this extraembryonic tissue (Sasaki et al., 2016; Ma et al., 2019; Xiang et al., 2020; Yang et al., 2021). It was also reported that BAP induces amnion rather than trophoblast fate in human primed ESCs (Guo et al., 2021; Io et al., 2021). Therefore, we examined amniotic properties in AP-treated cells on day 2, a time point when BMP4 expression peaks (Figure 3C). Morphological changes suggestive of a transition from columnar to squamous epithelium, an anatomical feature distinguishing amniotic ectoderm from the epiblast (Figure S4A; Luckett et al., 1975; Shao et al., 2017a, 2017b; Xiang et al., 2020), were observed in these cells (Figures 4A–4C). The squamous epithelium was negative for NANOG, but coexpressed low levels of OCT3/4 and TFAP2A (Figure 4D), as seen in the primate early amnion epithelium or human amniogenesis model using stem cells (Shao et al., 2017a, Shao et al., 2017b; Xiang et al., 2020; Zheng et al., 2019; Zhu et al., 2020). Next, the AP-treated cells were compared with previously reported ESC-derived amnion-like cells (Shao et al., 2017a-). Hierarchical clustering and correlation scoring indicated that, on day 2, the AP-treated cells had the highest transcriptional similarity with the amnion-like cells (Figures 4E and S4B). Indeed, most of the genes whose expression was upregulated in the amnion-like cells were also induced in the AP-treated cells (Figures 4F, S4C, and S4D). They included genes such as *ISL1* and *HAND1*, which have been reported to express in the primate amnion (Knöfler et al., 2002; Ma et al., 2019; Yang et al., 2021). Immunostaining showed that the majority of cells expressed these proteins at this time point (Figures 4G and 4H). As expected from the transcriptome similarity, AP treatment in the three-dimensional environment steered primed ESCs to form a cystic morphology resembling that of the reported amnion-like cells (Shao et al., 2017a-; Figures S4E and S4F). Furthermore, when compared at a single-cell resolution with the embryonic sac, an *in vitro* model recapitulating human post-implantation development and cell allocation (Zheng et al., 2019), AP-treated cells were plotted closer to the amniotic analogous of the embryonic sac (Figure 4I).

Collectively, these results suggested that human primed ESCs give rise to the cells that share a set of cytological and transcriptional features with nascent amniotic ectoderm at an early phase of AP-induced differentiation.

Coexistence of late amnion-like cells and STB-like cells

The mRNA expression of BMP4 and ISL1 immediately returned to the basal level, but some amnion genes, such as *HAND1* and *WNT6*, were still expressed on day 4, a time point when STB-like cells appeared (Figure S4C). Intriguingly, HAND1 protein level seemed to drop in the cells that started expressing CGβ (Figure S5A, arrowhead). Indeed, the single-cell transcriptome analyses revealed that the expression level of *HAND1* mRNA remained high in cells that did not express *CGA* or *SDC1* (Figures 5A, 2B, and S2B). The mutually exclusive pattern of HAND1 and SDC1 expression were also seen at a protein level (Figure 5C). When looking into DEGs between HAND1$^+$ and SDC1$^+$ populations, the expression level of genes reported to be specific to human amniotic ectodermal cells (*GABRP*, *VTCN1*, *IGFBP3*, and so on; Roost et al., 2015; Zhu et al., 2020, Tyser et al., 2021) were high in HAND1$^+$ cells but low in SDC1$^+$ cells (Figures 5D and S5B–S5D). Quantitative RT-PCR analyses indicated the significant elevation of the mRNA levels of these genes on day 4 of AP treatment (Figure S5E). We focused on VTCN1, whose expression was undetectable or low in the trophoblast lineages of the cultured human embryos (Xiang et al., 2020; Figure S6B), as a putative surface marker to distinguish the HAND1$^+$ cells from the SDC1-expressing population (Figures 5D and 5E). Flow cytometric analyses indicated that the half portion of the cells was positive for VTCN1 after 5 days of AP addition (Figure 5F). We then fractionated the GATA3$^+$ cells into VTCN-high and -low populations, and measured the expression level of amnion- or STB-related genes (for gating strategy, see Figure S5F). VTCN1-high cells express higher level of amnion-related genes, while VTCN1-low cells expressed STB-related genes at a high level (Figure 5G), supporting the results from scRNA-seq analyses. In the aspect of immunological features, class I HLA expression was retained in VCTN1-positive cells, while PD-L1 induction was observed only in the

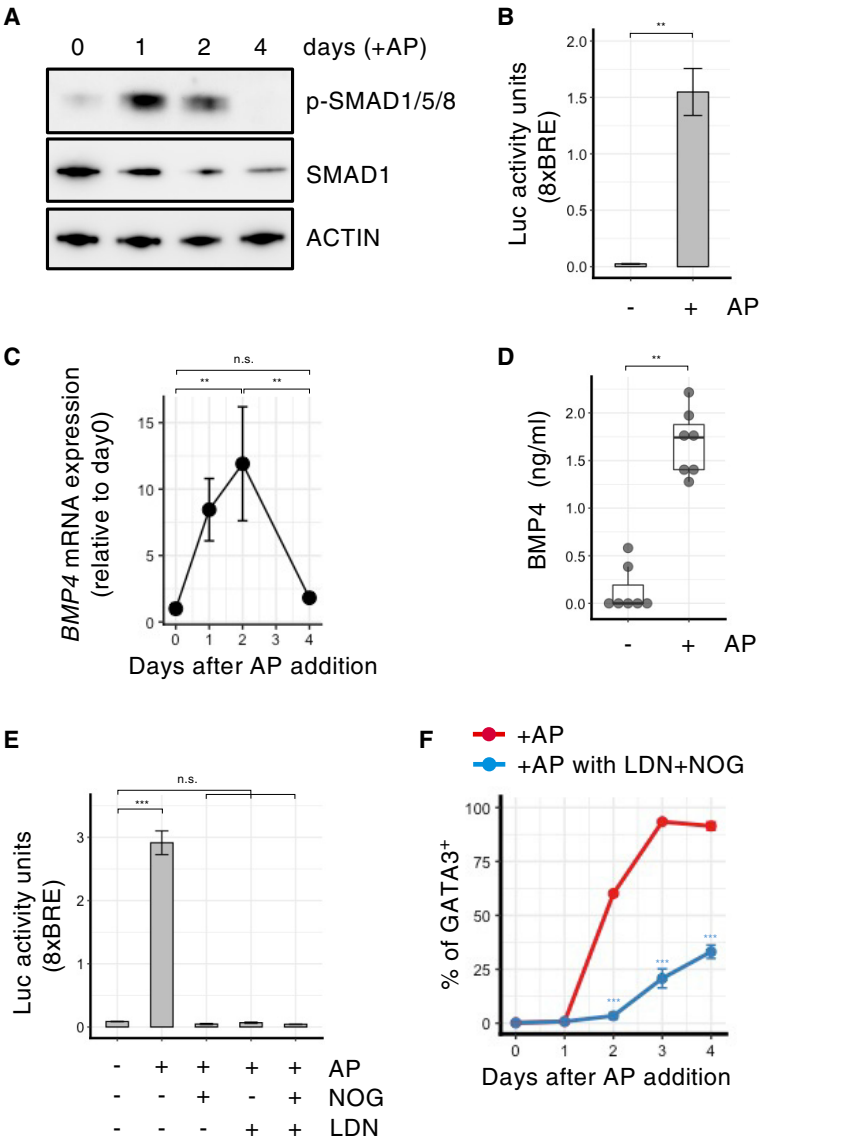

Figure 3. Molecular analyses of ESC-to-GATA3$^+$ ExE conversion

(A) Western blotting analyses for the SMAD signaling pathway at the indicated timepoints of AP-induced differentiation. Actin was examined as a loading control. Representatives from three independent experiments are shown.

(B) Luciferase activity measurement using the 8×BRE reporter plasmid before and after AP addition. Data represent the mean with SD (n = 3).

(C) qPCR assay for BMP4. Cells were treated with AP for the indicated periods. Data represent the mean with SD (n = 3).

(D) Secretion levels of BMP4 in culture supernatants (day 3). Data represent the mean with SD (n = 7).

(E) Inhibitory effects of NOG and LDN on BMP-dependent transcription. Luciferase activity was measured before and after AP addition (day 2). Data represent the mean with SD (n = 3).

(F) Time course quantitation of GATA3$^+$ cells in the presence and absence of BMP blockers. Data represent the mean with SD (n = 3).

(G) Immunostaining of KhES-1 cells for the indicated lineage markers. Representatives from three independent experiments are shown. Scale bars, 100 μm. Statistical analyses were done by paired t test (B and E), Tukey's test among all groups (C), Wilcoxon signed-rank test for paired data (D), unpaired Student's t test versus control cells at each time point (F); N.D., not detected; n.s., not significant; *p < 0.05, **p < 0.01, ***p < 0.001. See also Figure S3.

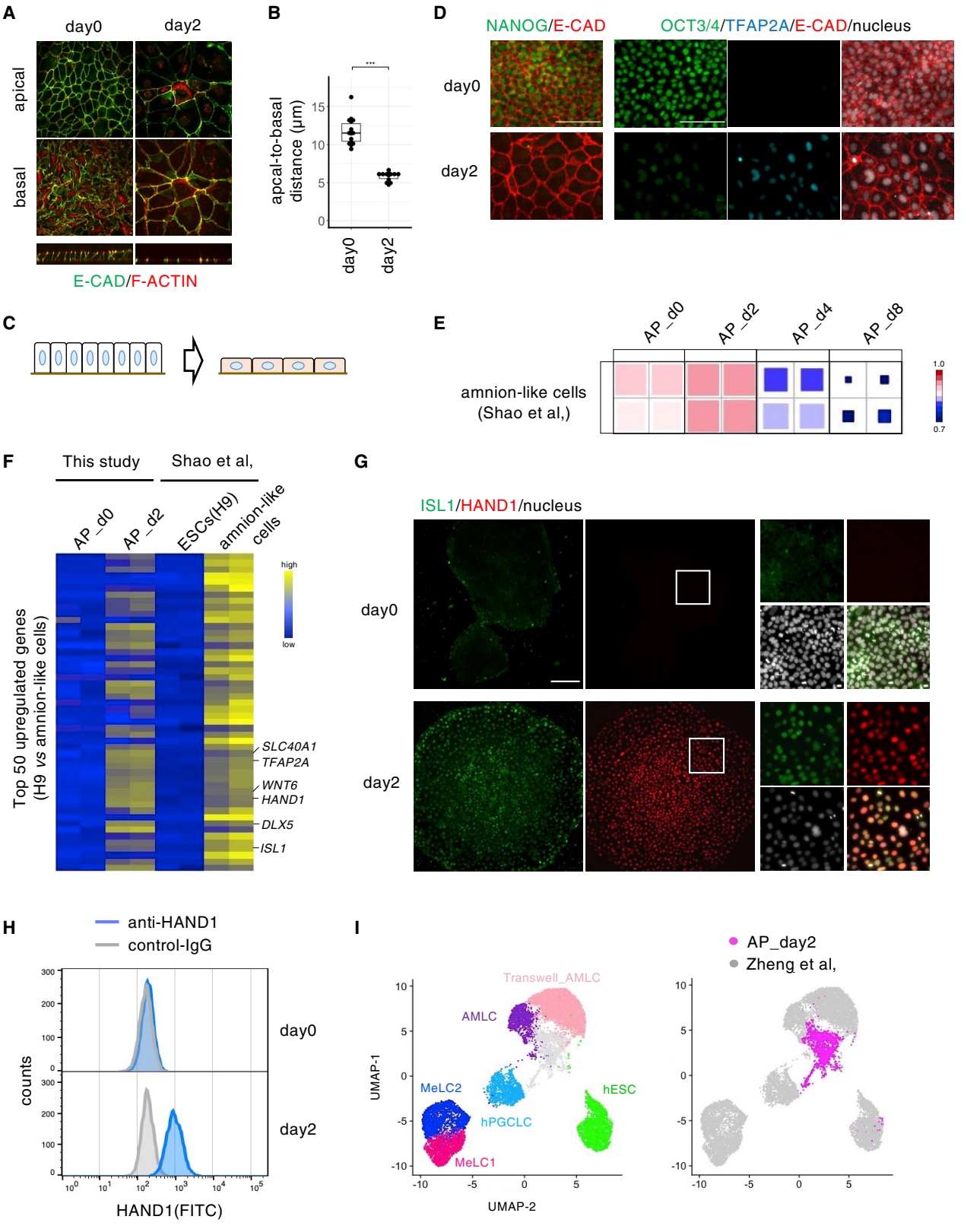

(legend on next page)

HAND1-negative areas (Figure S5G). Consistent with the low expression of fusogenic genes in HAND1$^+$ cells (Figure 2F, D4_clst_0, _1, and _2), syncytia were not induced in these cells (Figure S5H).

Cell fate specification is defined by cell-type-specific gene regulatory networks (GRNs) that are under the control of transcription factor binding to *cis*-regulatory elements of target genes. To verify the VTCN1$^+$ and SDC1$^+$ cells at a gene regulatory level, we analyzed GRNs by SCENIC (Aibar et al., 2017). These analyses revealed that the pattern of GRN activity in cluster 4 was clearly distinct from that in other clusters (Figure 5H). Of note, cluster 4 cells showed higher activity of GRNs governed by GATA2, TFAP2C, and TBX3, all of which were previously reported to activate trophoblast- or STB-related programs (Figure 5I) (Krendl et al., 2017; Lv et al., 2019). Cluster 0 and 1, which included HAND1$^+$/VTCN$^+$ cells, showed lower activity of these GRNs but higher activity of different classes of GRNs (Figure 5I).

On the basis of these definite differences in gene expression, cytological features, and GRNs, we concluded that two distinct types of cells, one showing STB-like phenotypes and the other resembling late amnion ectoderm, were induced simultaneously in the later stages of AP-induced differentiation.

Branching of STB-like cells from amnionic differentiation trajectory

As described, we observed stepwise transitions into the two different states of GATA3-expressing cells. To decipher the temporal dynamics of cell state transitions from day 2–4, we interrogated the integrated single-cell transcriptome dataset (Figure 6A). Computing pseudotime of each cell postulated putative differentiation trajectory during this period, and advocated some branches of the trajectory (Figure 6B). We focused on a branching point where the trajectory bifurcated into SDC1$^+$ and VTCN1$^+$ cells (Figures 6B and S6A; the branching point is indicated by an arrow in Figure 6B). We omitted outlier cells and classified the remaining cells into three populations based on this branching point, one as a pre-branching (ExE-A), and the other two as post-branching (ExE-B and ExE-C) (Figure 6C). The identity of cells from each group was assessed by comparing them with cells from implantation-stage and gastrulation-stage human embryos (Xiang et al., 2020; Tyser et al., 2021). We first ascertained the tissue distribution of the marker genes used in the previous analyses (Figure S6B). Uniform Manifold Approximation and Projection (UMAP) projection of the AP-treated cells together with these reference cells revealed a unique nature of the AP-induced differentiation route (Figures 6D and S6C). ExE-A cells were in close proximal to the embryonic pluripotent population and ExE-B cells partially overlapped with the cells annotated as ectoderm (amniotic/embryonic). ExE-C cells delaminated from the trajectory to approach the cells annotated as STB. The comparison of the expression of lineage-specific genes also indicated that ExE-A and ExE-B cells showed similar trends to embryonic/amniotic ectoderm, while ExE-C cells shared highly expressed genes with trophoblasts, especially STBs (Figure 6E). Consistent with these results, the signature scores calculated using amnion tissue-enriched genes increased with the progression from ExE-A to ExE-B, while the scores for the STB signature remained at a basal level (Figures 6F, 6G, and S6D). In the transition from ExE-A to ExE-C, we observed the opposite pattern of signature score dynamics (Figures 6F, 6G, and S6E show expression dynamics of the selected genes). SCENIC analyses indicated that ISL1, which has been reported to be active in early amnion of cynomolgus monkey (Yang et al., 2021), showed a higher level of activity in the ExE-A cells (Figures 6H, S6F, and S6G). On the other hand, the ISL1 activity declined in the ExE-C cells. These data suggest that the ExE-A to ExE-B transition recapitulates the progression of early to late amniotic ectoderm, and that the ExE-C cells arise from the trajectory of amniotic differentiation. To confirm this, we tracked cell divisions from day 2 by live imaging, and characterized the fate of the descendants arising from the same cells by endpoint immunostaining (Figures 6I–6K and Video S3). This experiment showed that both SDC1$^+$ cells and VTCN1$^+$ cells were observed in the same clonal population, indicating that they arise from the common origin.

Taken altogether, these results suggested that STB-like cells are segregated from the cells undergoing differentiation from the epiblast to amniotic ectodermal lineage (Figure S6H).

DISCUSSION

Human ESCs are known to acquire certain trophoblast characteristics in response to BMP ligands, but the trophoblast identity of the

Figure 4. Amniotic features at the early phase of differentiation

(A) Confocal images of the KhES-1 colonies treated or untreated with AP for 2 days. The upper and middle panels are the x-y views at apical and basal sections, respectively. The low is the y-z view. Scale bar, 100 μm.

(B) Comparison of apical-basal distances of AP-treated or -untreated colonies (10 different images from three independent experiments).

(C) Schematic diagram of the morphological transition (y-z view) of the AP-treated colony.

(D) Immunostaining of KhES-1 cells before or after treatment with AP for the indicated proteins. Scale bar, 100 μm.

(E and F) Comparison of transcriptomes from AP-treated KhES-1 cells with the published ones from amnion-like cells (Shao et al., 2017a-). (E) Spearman correlation. (F) Heatmap representation in AP-treated or -untreated cells using the top 50 genes (logFC values) that were shown to be upregulated in the amnion-like cells. The examples for amnion-related genes are indicated.

(G) Immunostaining of AP-treated KhES-1 cells for the indicated proteins. Faint fluorescence for ISL-1 were detected before AP addition, but they were non-nucleus. Right panels are enlarged images of the region enclosed in the center images. Scale bars, 100 μm.

(H) Flow cytometry panels for the quantification of HAND1- expression in KhES-1 cells before and after treatment with AP for 2 days. As a negative control, cells were incubated without a primary antibody and then stained using an FITC-conjugated mouse IgG antibody. Representative histograms from three independent experiments are shown.

(I) UMAP projection of AP-treated KhES-1 cells (day 2) using cells from the *in vitro* models for human embryonic sac as a reference (Zheng et al., 2019). Cell annotations follow the original report: AMLC, amnion-like cell; Transwell-AMLC, AMLC derived by the Transwell method; hPGCLC, human primordial germ cell-like cell; MeLC1-2, mesoderm-like cell. See also Figure S4.

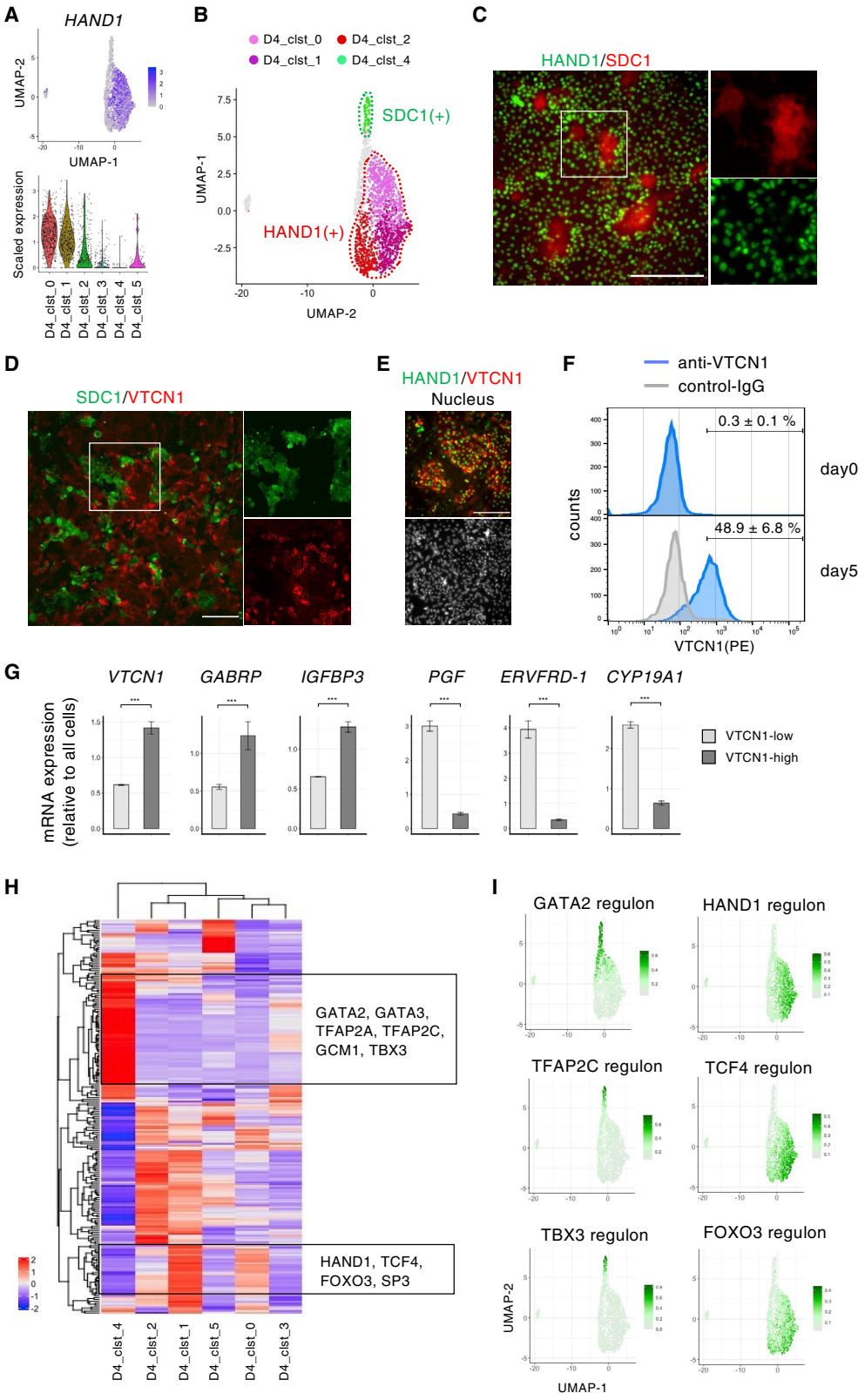

(legend on next page)

ESC derivatives is often questionable. Some reports have claimed that they represent non-trophoblastic cells, such as amnionic derivatives (Bernardo et al., 2011; Guo et al., 2021; Io et al., 2021). Considering the controversial situation, we avoided referring to the AP-induced cells as trophoblasts. Instead, we referred to them as GATA3$^+$ ExE cells, and characterized them extensively.

We demonstrated that AP-treated cells start to express early amnion-related genes in the early phase of differentiation, including *BMP4* and *ISL1*. The cells expressing these genes are functionally crucial for the subsequent steps of differentiation, because the inhibition of the BMP4 action impedes the increase of GATA3$^+$ cells. The expression levels of these genes decreased with prolonged culture, but instead genes reported to be induced in the later stage of primate amniogenesis (e.g., *VTCN1*, *GABRP*, and *IGFBP3*) began to be expressed specifically in cells retaining HAND1 expression. When compared with cells from the human embryos, the HAND1$^+$/VTCN$^+$ population is most closely matched with cells from the amnion tissue of the gastrulating embryos. These observations suggested that our differentiation system represents the process of amnion differentiation from the epiblast, which agrees with previous reports (Guo et al., 2021; Io et al., 2021). An important aspect of this study is that STB-like cells are also induced in the same culture. These cells shared a series of cellular properties with authentic STBs, including endocrine functions, immunological features, characteristic syncytial morphology, and underlying GRN activity, and were clearly distinguished from the HAND1$^+$/VTCN1$^+$ late amnion-like cells. Trajectory analyses and cell tracking by live imaging indicated that these two cell types emerged from the same origin, supporting the idea that AP-induced differentiation bifurcated into different trajectories leading to distinct types of extraembryonic cells (Figure S6H). We supposed that the AP-induced STB-like cells are phenotypically equivalent to the BAP-induced ones (Xu et al., 2002; Yabe et al., 2016), but the elimination of exogenous BMP ligands from the culture conditions sheds light on the cell-autonomous role of BMP4 in the fate specification to extraembryonic lineages.

Finally, we discuss the biological implications of the differentiation of STB-like cells from the ESCs with primed pluripotency. Why conventional ESCs, which are regarded as counterparts of the post-implantation epiblast, give rise to trophoblast-like cells has been a big question since the first report by Thompson's group (Xu et al., 2002). Recent progress in primate embryology has unveiled substantial differences between mouse and human development (Nakamura et al., 2016; Petropoulos et al., 2016; Rossant and Tam, 2017; Turco and Moffett, 2019) and offers another possibility for this long-standing question. Considered together with accumulating transcriptome information on early primate embryos, the results presented in this study provide the possibility that, in primates, the amniotic ectoderm serves as another source for placental hormone-producing syncytia. Although the presence of such amniotic ectoderm-derived cells within the primitive syncytium *in vivo* remains ambiguous, it has been reported that CGβ-expressing cells are located proximal to the amniotic epithelium of the cultured human embryos (Xiang et al., 2020). Whether the syncytium-forming extraembryonic cells originated not only from the trophectodermal lineages but also from the amniotic ectoderm, and whether they function together to support the growth of the primate fetus, are exciting questions that challenge the conventional view of mammalian development. Future *in vivo* investigations utilizing strict lineage tracing techniques will help us to discuss the hypothesis.

Limitations of the study

The early stage of differentiation from human ESCs may recapitulate developmental processes that corresponds to the post-implantation stage of human embryonic development. However, our current knowledge of cellular dynamics around the implantation stage is still insufficient, making it difficult to accurately evaluate the reliability of the *in vitro* model. We and other groups have utilized a few previously published scRNA-seq data from the human or non-human primate embryos, but the molecular information of the early amniotic ectoderm is limited, perhaps because the number of amniotic cells was very low in these previous analyses. It is currently uncertain whether STB-like cells arise from the post-implantation epiblasts *in vivo*.

STAR★METHODS

Detailed methods are provided in the online version of this paper and include the following:

- KEY RESOURCES TABLE
- RESOURCE AVAILABILITY
  - Lead contact
  - Materials Availability
  - Data and code availability
- EXPERIMENTAL MODEL AND SUBJECT DETAILS
  - Pluripotent stem cells
- METHOD DETAILS

Figure 5. Coexistence of late amnion-like cells and STB-like cells

(A) UMAP and violin plot representations of expression profile of *HAND1* at day4. Cell clusters are the same as those in Figure 2A.

(B) Cluster distribution of HAND1+ or SDC1+ cells.

(C–E) Immunostaining of KhES-1 cells treated with AP for 5 days. Mutual exclusive expression of HAND1 and SDC1 (C, scale bar, 200 μm) or VTCN1 and SDC1 (D, scale bar, 100 μm), and colocalized expression of HAND1 and VTCN1 (E, scale bar, 200 μm) are shown. Right panels are enlarged images of the region enclosed in the left images (C and D).

(F) Flow cytometry panels for the quantification of VTCN1 expression in KhES-1 cells before and after treatment with AP for 5 days. As a negative control, cells were stained using a PE-conjugated mouse IgG antibody. Representative histograms from three independent experiments are shown.

(G) qPCR assay for evaluating differential gene expression between VTCN1-low and -high cells. KhES-1 cells treated with AP for 5 days were divided by a flow cytometer into two populations according to the expression level of VTCN1. Gene expressions are shown relative to non-sorted total cells with SD (n = 3).

(H and I) GRN analyses in AP-treated cells (day 4). (H) Heatmap representation of the GRN activity. (I) The activity plotting of the selected regulons on UMAP space. Distribution of regulons enriched in cluster 4 (left) and in cluster 0/1 (right). Statistical analyses were done by paired t test (G); ***$p < 0.001$. See also Figure S5.

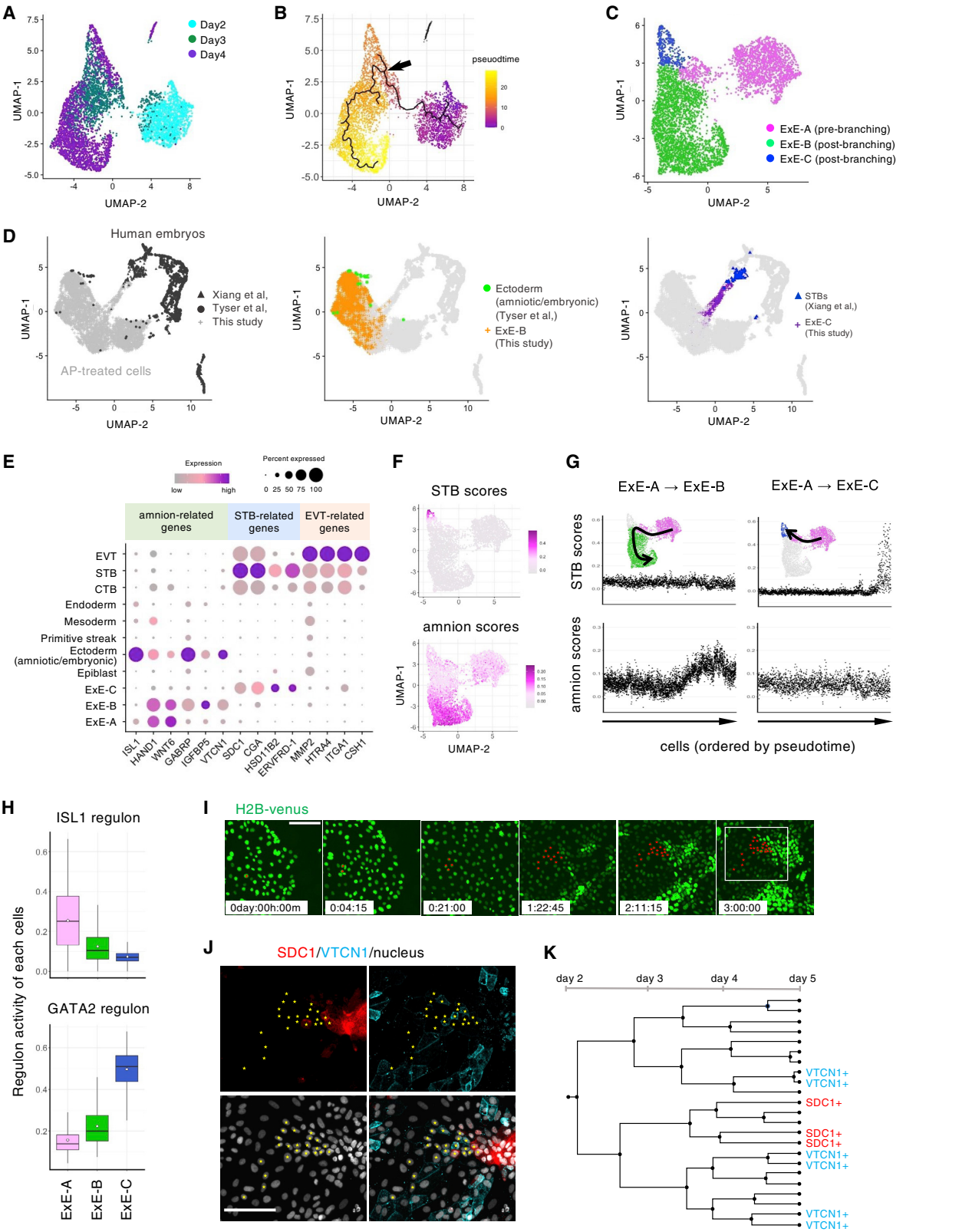

(legend on next page)

- Plasmids and transfection procedure
- Generation of GATA3 reporter cell line
- GATA3^{+} ExE differentiation
- Immunostaining
- Western blot analyses
- Flow cytometry analyses
- Luciferase reporter assays
- Quantitative real-time PCR
- Live imaging
- Capture of syncytia formation
- Bulk-RNA sequence and data analyses
- Single-cell RNA sequence and data analyses
- SCENIC- analyses
- External data
- Graphical presentation

● QUANTIFICATION AND STATISTICAL ANALYSIS

SUPPLEMENTAL INFORMATION

Supplemental information can be found online at https://doi.org/10.1016/j.celrep.2022.110973.

ACKNOWLEDGMENTS

We are grateful to Liaison Laboratory Research Promotion Center (LILA) at IMEG, Kumamoto University, and Single-Cell Genome Information Analysis Core (SignAC) at WPI-ASHBi, Kyoto University, for sequencing; K. Yusa for a hyperactive PBase vector; H. Niwa, K. Matsuura, Y. Seto, and R. Tsutsumi for experimental support, discussions, and fruitful comments on the manuscript; T. Tsukiyama, M. Mutou, and M. Ema for discussions; and A. Ohgushi and all members of our laboratory for support and encouragement. We also express special thanks to Yoshiki Sasai with respect to his legacy in science. This work was supported by the Program for Technological Innovation of Regenerative Medicine, Research Center Network for Realization of Regenerative Medicine from the Japan Agency for Medical Research and Development (17bm0704013h9902); Takeda Science Foundation; the Mochida Memorial Foundation for Medical and Pharmaceutical Research; Joint Usage/Research Center for Developmental Medicine, IMEG, Kumamoto University; ISHIZUE 2020 of Kyoto University Research Development Program; and INFRONT Office of Directors' Research Grants Program (to M.O.); and was partially supported by Grant-in-Aid for Scientific Research on Innovative Areas (Ministry of Education, Culture, Sports, Science and Technology, Japan (JSPS) (16H06480 to M.E.); and Core Research for Evolutional Science and Technology (CREST, JST) (JPMJCR12W2 to M.E.).

AUTHOR CONTRIBUTIONS

M.O. designed the project, performed experiments and data analyses, and wrote the manuscript. N.T. helped with library preparation for scRNA-seq. A.V. and M.E. supported M.O. in data analyses.

DECLARATION OF INTERESTS

The authors declare no competing interests.

Received: July 15, 2021
Revised: March 21, 2022
Accepted: May 24, 2022
Published: June 21, 2022

REFERENCES

Aibar, S., and Aerts, S.Laboratory of Computational Biology; VIB-KU Leuven Center for Brain & Disease Research (2016a). RcisTarget: identify transcription factor binding motifs enriched on a gene list. R/Bioconductor package. https://bioconductor.org/packages/3.12/bioc/html/RcisTarget.html.

Aibar, S., and Aerts, S.Laboratory of Computational Biology; VIB-KU Leuven Center for Brain & Disease Research (2016b). AUCell: analysis of 'gene set' activity in single-cell RNA-seq data. https://bioconductor.org/packages/3.12/bioc/html/AUCell.html.

Aibar, S., González-Blas, C.B., Moerman, T., Huynh-Thu, V.A., Imrichova, H., Hulselmans, G., Rambow, F., Marine, J.C., Geurts, P., Aerts, J., et al. (2017). SCENIC: single-cell regulatory network inference and clustering. Nat. Methods *14*, 1083–1086. https://doi.org/10.1038/nmeth.4463.

Amita, M., Adachi, K., Alexenko, A.P., Sinha, S., Schust, D.J., Schulz, L.C., Roberts, R.M., and Ezashi, T. (2013). Complete and unidirectional conversion of human embryonic stem cells to trophoblast by BMP4. Proc. Natl. Acad. Sci. U S A *110*, E1212–E1221. https://doi.org/10.1073/pnas.1303094110.

Bernardo, A.S., Faial, T., Gardner, L., Niakan, K.K., Ortmann, D., Senner, C.E., Callery, E.M., Trotter, M.W., Hemberger, M., Smith, J., et al. (2011). BRACHYURY and CDX2 mediate BMP-induced differentiation of human and mouse pluripotent stem cells into embryonic and extraembryonic lineages. Cell Stem Cell *9*, 144–155. https://doi.org/10.1016/j.stem.2011.06.015.

Cao, J., Spielmann, M., Qiu, X., Huang, X., Ibrahim, D.M., Hill, A.J., Zhang, F., Mundlos, S., Christiansen, L., Steemers, F.J., et al. (2019). The single-cell transcriptional landscape of mammalian organogenesis. Nature *566*, 496–502. https://doi.org/10.1038/s41586-019-0969-x.

Cao, J., O'Day, D.R., Pliner, H.A., Kingsley, P.D., Deng, M., Daza, R.M., Zager, M.A., Aldinger, K.A., Blecher-Gonen, R., Zhang, F., et al. (2020). A human cell atlas of fetal gene expression. Science *370*, eaba7721. https://doi.org/10.1126/science.aba7721.

Figure 6. Branching of STB-like cells from amnionic differentiation trajectory

(A) UMAP representation of the cells treated with AP for 2 days (1,949), 3 days (1,978), and 4 days (2,149 cells).

(B) Cellular trajectory reconstruction using Monocle3. Color gradient represents the transition of computed pseudotimes. Black lines show the estimated trajectory and arrow indicates a branching point we focus on.

(C) UMAP rebuilt using 5,039 cells. Cells were classified into three groups as indicated.

(D and E) Comparison of AP-treated cells with from the implantation stage (Xiang et al., 2020, shown as triangles) and gastrulation stage of human embryos (Tyser et al., 2021, shown as circles). (D) UMAP projection of AP-treated cells using these embryonic cells as a reference. (E) Dot plot representation for expression pattern of the lineage-specific genes. Cell annotations were followed to the original reports.

(F) Signature score distribution. Signature scores were calculated using genes shown to be enriched in early STBs of the cultured human embryos (Xiang et al., 2020) or the amnion tissue of cynomolgus monkey embryos (Ma et al., 2019). They are shown on the UMAP space.

(G) Pseudotime-dependent dynamics of signature scores along with each trajectory.

(H) Boxplot presentation of the regulon activities for each cell. The regulons governed by ISL1 (upper) and GATA2 (bottom) are shown.

(I–K) Clonal analyses for differentiation trajectories. (I) KhES-1 cells expressing H2B-Venus were treated with AP for 2 days, and then their division histories were traced by live imaging. (J) At day 5, the identity of descendant cells was characterized by immunostaining. Red and yellow stars indicate the clones originated from the same cell. (K) Lineage tree of the marked cells. Scale bars, 100 μm. See also Figure S6 and Video S3.

Cliff, T.S., Wu, T., Boward, B.R., Yin, A., Yin, H., Glushka, J.N., Prestegaard, J.H., and Dalton, S. (2017). MYC controls human pluripotent stem cell fate decisions through regulation of metabolic flux. Cell Stem Cell *21*, 502–516.e9. https://doi.org/10.1016/j.stem.2017.08.018.

Dobin, A., Davis, C.A., Schlesinger, F., Drenkow, J., Zaleski, C., Jha, S., Batut, P., Chaisson, M., and Gingeras, T.R. (2013). STAR: ultrafast universal RNA-seq aligner. Bioinformatics *29*, 15–21. https://doi.org/10.1093/bioinformatics/bts635.

Galili, T., O'Callaghan, A., Sidi, J., and Sievert, C. (2018). heatmaply: an R package for creating interactive cluster heatmaps for online publishing. Bioinformatics *34*, 1600–1602. https://doi.org/10.1093/bioinformatics/btx657.

Guo, G., Stirparo, G.G., Strawbridge, S.E., Spindlow, D., Yang, J., Clarke, J., Dattani, A., Yanagida, A., Li, M.A., Myers, S., et al. (2021). Human naïve epiblast cells possess unrestricted lineage potential. Cell Stem Cell *28*, 1040–1056.e6. https://doi.org/10.1016/j.stem.2021.02.025.

Hao, Y., Hao, S., Andersen-Nissen, E., Mauck, W.M., 3rd, Zheng, S., Butler, A., Lee, M.J., Wilk, A.J., Darby, C., Zager, M., et al. (2021). Integrated analysis of multimodal single-cell data. Cell *184*, 3573–3587.e29. https://doi.org/10.1016/j.cell.2021.04.048.

Huang, K., Zhu, Y., Ma, Y., Zhao, B., Fan, N., Li, Y., Song, H., Chu, S., Ouyang, Z., Zhang, Q., et al. (2018). BMI1 enables interspecies chimerism with human pluripotent stem cells. Nat. Commun. *9*, 4649. https://doi.org/10.1038/s41467-018-07098-w.

Huynh-Thu, V.A., Irrthum, A., Wehenkel, L., and Geurts, P. (2010). Inferring regulatory networks from expression data using tree-based methods. PLoS One *5*, e12776. https://doi.org/10.1371/journal.pone.0012776.

Horii, M., Morey, R., Bui, T., Touma, O., Nelson, K.K., Cho, H.Y., Rishik, H., Laurent, L.C., and Parast, M.M. (2021). Modeling preeclampsia using human induced pluripotent stem cells. Sci. Rep. *11*, 5877. https://doi.org/10.1038/s41598-021-85230-5.

Io, S., Kabata, M., Iemura, Y., Semi, K., Morone, N., Minagawa, A., Wang, B., Kojima, Y., Iwatani, C., Tsuchiya, H., et al. (2021). Capturing human trophoblast development with naïve pluripotent stem cells *in vitro*. Cell Stem Cell *28*, 1023–1039.e13. https://doi.org/10.1016/j.stem.2021.03.013.

Jain, A., and Tuteja, G. (2019). TissueEnrich: tissue-specific gene enrichment analysis. Bioinformatics *35*, 1966–1967. https://doi.org/10.1093/bioinformatics/bty890.

Kawase, E., Takada, K., Nakatani, R., Yamazaki, S., and Suemori, H. (2021). Generation of clinical-grade human embryonic stem cell line KthES11 according to Japanese regulations. Stem Cell Res. *54*, 102383. https://doi.org/10.1016/j.scr.2021.102383.

Kang, Y., Ai, Z., Duan, K., Si, C., Wang, Y., Zheng, Y., He, J., Yin, Y., Zhao, S., Niu, B., et al. (2018). Improving cell survival in injected embryos allows primed pluripotent stem cells to generate chimeric cynomolgus monkeys. Cell Rep. *25*, 2563–2576.e9. https://doi.org/10.1016/j.celrep.2018.11.001.

Krendl, C., Shaposhnikov, D., Rishko, V., Ori, C., Ziegenhain, C., Sass, S., Simon, L., Müller, N.S., Straub, T., Brooks, K.E., et al. (2017). GATA2/3-TFAP2A/C transcription factor network couples human pluripotent stem cell differentiation to trophectoderm with repression of pluripotency. Proc. Natl. Acad. Sci. U S A *114*, E9579–E9588. https://doi.org/10.1073/pnas.1708341114.

Knöfler, M., Meinhardt, G., Bauer, S., Loregger, T., Vasicek, R., Bloor, D.J., Kimber, S.J., and Husslein, P. (2002). Human Hand1 basic helix-loop-helix (bHLH) protein: extra-embryonic expression pattern, interaction partners and identification of its transcriptional repressor domains. Biochem. J. *361*, 641–651. https://doi.org/10.1042/bj3610641.

Li, B., and Dewey, C.N. (2011). RSEM: accurate transcript quantification from RNA-Seq data with or without a reference genome. BMC Bioinf. *12*, 323. https://doi.org/10.1186/1471-2105-12-323.

Luckett, W.P. (1975). The development of primordial and definitive amniotic cavities in early Rhesus monkey and human embryos. Am. J. Anat. *144*, 149–167. https://doi.org/10.1002/aja.1001440204.

Lv, B., An, Q., Zeng, Q., Zhang, X., Lu, P., Wang, Y., Zhu, X., Ji, Y., Fan, G., and Xue, Z. (2019). Single-cell RNA sequencing reveals regulatory mechanism for trophoblast cell-fate divergence in human peri-implantation conceptuses. PLoS Biol. *17*, e3000187. https://doi.org/10.1371/journal.pbio.3000187.

Ma, H., Zhai, J., Wan, H., Jiang, X., Wang, X., Wang, L., Xiang, Y., He, X., Zhao, Z.A., Zhao, B., et al. (2019). In vitro culture of cynomolgus monkey embryos beyond early gastrulation. Science *366*, eaax7890. https://doi.org/10.1126/science.aax7890.

Martello, G., and Smith, A. (2014). The nature of embryonic stem cells. Annu. Rev. Cell Dev. Biol. *30*, 647–675. https://doi.org/10.1146/annurev-cellbio-100913-013116.

Nakagawa, M., Koyanagi, M., Tanabe, K., Takahashi, K., Ichisaka, T., Aoi, T., Okita, K., Mochiduki, Y., Takizawa, N., and Yamanaka, S. (2008). Generation of induced pluripotent stem cells without Myc from mouse and human fibroblasts. Nat. Biotechnol. *26*, 101–106. https://doi.org/10.1038/nbt1374.

Nakamura, T., Okamoto, I., Sasaki, K., Yabuta, Y., Iwatani, C., Tsuchiya, H., Seita, Y., Nakamura, S., Yamamoto, T., and Saitou, M. (2016). A developmental coordinate of pluripotency among mice, monkeys and humans. Nature *537*, 57–62. https://doi.org/10.1038/nature19096.

Nichols, J., and Smith, A. (2009). Naive and primed pluripotent states. Cell Stem Cell *4*, 487–492. https://doi.org/10.1016/j.stem.2009.05.015.

Ohgushi, M., Matsumura, M., Eiraku, M., Murakami, K., Aramaki, T., Nishiyama, A., Muguruma, K., Nakano, T., Suga, H., Ueno, M., et al. (2010). Molecular pathway and cell state responsible for dissociation-induced apoptosis in human pluripotent stem cells. Cell Stem Cell *7*, 225–239. https://doi.org/10.1016/j.stem.2010.06.018.

Ohgushi, M., Minaguchi, M., and Sasai, Y. (2015). Rho-signaling-directed YAP/TAZ activity underlies the long-term survival and expansion of human embryonic stem cells. Cell Stem Cell *17*, 448–461. https://doi.org/10.1016/j.stem.2015.07.009.

Okae, H., Toh, H., Sato, T., Hiura, H., Takahashi, S., Shirane, K., Kabayama, Y., Suyama, M., Sasaki, H., and Arima, T. (2018). Derivation of human trophoblast stem cells. Cell Stem Cell *22*, 50–63.e6. https://doi.org/10.1016/j.stem.2017.11.004.

Petropoulos, S., Edsgärd, D., Reinius, B., Deng, Q., Panula, S.P., Codeluppi, S., Plaza Reyes, A., Linnarsson, S., Sandberg, R., and Lanner, F. (2016). Single-cell RNA-seq reveals lineage and X chromosome dynamics in human preimplantation embryos. Cell *165*, 1012–1026. https://doi.org/10.1016/j.cell.2016.03.023.

Roberts, R.M., Ezashi, T., Sheridan, M.A., and Yang, Y. (2018). Specification of trophoblast from embryonic stem cells exposed to BMP4. Biol. Reprod. *99*, 212–224. https://doi.org/10.1093/biolre/ioy070.

Roberts, R.M., Loh, K.M., Amita, M., Bernardo, A.S., Adachi, K., Alexenko, A.P., Schust, D.J., Schulz, L.C., Telugu, B.P.V.L., Ezashi, T., and Pedersen, R.A. (2014). Differentiation of trophoblast cells from human embryonic stem cells: to be or not to be? Reproduction *147*, D1–D12. https://doi.org/10.1530/REP-14-0080.

Robinson, M.D., McCarthy, D.J., and Smyth, G.K. (2010). edgeR: a Bioconductor package for differential expression analysis of digital gene expression data. Bioinformatics *26*, 139–140. https://doi.org/10.1093/bioinformatics/btp616.

Roost, M.S., van Iperen, L., Ariyurek, Y., Buermans, H.P., Arindrarto, W., Devalla, H.D., Passier, R., Mummery, C.L., Carlotti, F., de Koning, E.J., et al. (2015). KeyGenes, a tool to probe tissue differentiation using a human fetal transcriptional atlas. Stem Cell Rep. *4*, 1112–1124. https://doi.org/10.1016/j.stemcr.2015.05.002.

Rossant, J., and Tam, P.P.L. (2017). New insights into early human development: lessons for stem cell derivation and differentiation. Cell Stem Cell *20*, 18–28. https://doi.org/10.1016/j.stem.2016.12.004.

Rossant, J. (2018). Genetic control of early cell lineages in the mammalian embryo. Annu. Rev. Genet. *52*, 185–201. https://doi.org/10.1146/annurev-genet-120116-024544.

Sasaki, K., Nakamura, T., Okamoto, I., Yabuta, Y., Iwatani, C., Tsuchiya, H., Seita, Y., Nakamura, S., Shiraki, N., Takakuwa, T., et al. (2016). The germ

cell fate of cynomolgus monkeys is specified in the nascent amnion. Dev. Cell *39*, 169–185. https://doi.org/10.1016/j.devcel.2016.09.007.

Shao, Y., Taniguchi, K., Gurdziel, K., Townshend, R.F., Xue, X., Yong, K.M.A., Sang, J., Spence, J.R., Gumucio, D.L., and Fu, J. (2017a). Self-organized amniogenesis by human pluripotent stem cells in a biomimetic implantation-like niche. Nat. Mater. *16*, 419–425. https://doi.org/10.1038/nmat4829.

Shao, Y., Taniguchi, K., Townshend, R.F., Miki, T., Gumucio, D.L., and Fu, J. (2017b). A pluripotent stem cell-based model for post-implantation human amniotic sac development. Nat. Commun. *8*, 208. https://doi.org/10.1038/s41467-017-00236-w.

Sheridan, M.A., Yunusov, D., Balaraman, V., Alexenko, A.P., Yabe, S., Verjovski-Almeida, S., Schust, D.J., Franz, A.W., Sadovsky, Y., Ezashi, T., and Roberts, R.M. (2017). Vulnerability of primitive human placental trophoblast to Zika virus. Proc. Natl. Acad. Sci. U S A *114*, E1587–E1596. https://doi.org/10.1073/pnas.1616097114.

Sheridan, M.A., Yang, Y., Jain, A., Lyons, A.S., Yang, P., Brahmasani, S.R., Dai, A., Tian, Y., Ellersieck, M.R., Tuteja, G., et al. (2019). Early onset preeclampsia in a model for human placental trophoblast. Proc. Natl. Acad. Sci. U S A *116*, 4336–4345. https://doi.org/10.1073/pnas.1816150116.

Suemori, H., Yasuchika, K., Hasegawa, K., Fujioka, T., Tsuneyoshi, N., and Nakatsuji, N. (2006). Efficient establishment of human embryonic stem cell lines and long-term maintenance with stable karyotype by enzymatic bulk passage. Biochem. Biophys. Res. Commun. *345*, 926–932. https://doi.org/10.1016/j.bbrc.2006.04.135.

Taiyun, W., and Viliam, S. (2021). R package 'corrplot': visualization of a correlation matrix (version 0.90). https://github.com/taiyun/corrplot.

Turco, M.Y., and Moffett, A. (2019). Development of the human placenta. Development *146*, dev163428. https://doi.org/10.1242/dev.163428.

Tyser, R.C.V., Mahammadov, E., Nakanoh, S., Vallier, L., Scialdone, A., and Srinivas, S. (2021). Single-cell transcriptomic characterization of a gastrulating human embryo. Nature *600*, 285–289. https://doi.org/10.1038/s41586-021-04158-y.

Xiang, L., Yin, Y., Zheng, Y., Ma, Y., Li, Y., Zhao, Z., Guo, J., Ai, Z., Niu, Y., Duan, K., et al. (2020). A developmental landscape of 3D-cultured human pre-gastrulation embryos. Nature *577*, 537–542. https://doi.org/10.1038/s41586-019-1875-y.

Xu, R.H., Chen, X., Li, D.S., Li, R., Addicks, G.C., Glennon, C., Zwaka, T.P., and Thomson, J.A. (2002). BMP4 initiates human embryonic stem cell differentiation to trophoblast. Nat. Biotechnol. *20*, 1261–1264. https://doi.org/10.1038/nbt761.

Yabe, S., Alexenko, A.P., Amita, M., Yang, Y., Schust, D.J., Sadovsky, Y., Ezashi, T., and Roberts, R.M. (2016). Comparison of syncytiotrophoblast generated from human embryonic stem cells and from term placentas. Proc. Natl. Acad. Sci. U S A *113*, E2598–E2607. https://doi.org/10.1073/pnas.1601630113.

Yang, R., Goedel, A., Kang, Y., Si, C., Chu, C., Zheng, Y., Chen, Z., Gruber, P.J., Xiao, Y., Zhou, C., et al. (2021). Amnion signals are essential for mesoderm formation in primates. Nat. Commun. *12*, 5126. https://doi.org/10.1038/s41467-021-25186-2.

Yu, G., Wang, L.G., Han, Y., and He, Q.Y. (2012). clusterProfiler: an R package for comparing biological themes among gene clusters. OMICS *16*, 284–287. https://doi.org/10.1089/omi.2011.0118.

Yusa, K., Zhou, L., Li, M.A., Bradley, A., and Craig, N.L. (2011). A hyperactive piggyBac transposase for mammalian applications. Proc. Natl. Acad. Sci. U S A *108*, 1531–1536. https://doi.org/10.1073/pnas.1008322108.

Zheng, Y., Xue, X., Shao, Y., Wang, S., Esfahani, S.N., Li, Z., Muncie, J.M., Lakins, J.N., Weaver, V.M., Gumucio, D.L., and Fu, J. (2019). Controlled modelling of human epiblast and amnion development using stem cells. Nature *573*, 421–425. https://doi.org/10.1038/s41586-019-1535-2.

Zhu, Y., Wang, H., Yin, F., Guo, Y., Li, F., Gao, D., and Qin, J. (2020). Amnion-on-a-chip: modeling human amniotic development in mid-gestation from pluripotent stem cells. Lab Chip *20*, 3258–3268. https://doi.org/10.1039/d0lc00268b.

STAR★METHODS

KEY RESOURCES TABLE

REAGENT or RESOURCE	SOURCE	IDENTIFIER
Antibodies		
Mouse monoclonal anti-CD249	BD Biosciences	Cat#564532; RRID: AB_2738837
Mouse monoclonal anti-cytokeratin-7	DAKO	Cat#M7018; RRID: AB_2134589
Goat polyclonal anti-NANOG	R&D Systems	Cat#AF1997; RRID:AB_355097
Goat polyclonal anti-GATA3	R&D Systems	Cat#AF2605; RRID:AB_2108571
Rabbit polyclonal anti-OCT-4	Abcam	Cat#ab181557; RRID:AB_2687916
Mouse monoclonal anti-OCT3/4	BD Biosciences	Cat#611202; RRID:AB_398736
Rabbit polyclonal anti-TFAP2A	Abcam	Cat#ab52222; RRID:AB_867683
Rabbit polyclonal anti-TFAP2C	Sigma-Aldrich	Cat#HPA055179; RRID:AB_2686902
Rabbit polyclonal anti-VGLL1	Sigma-Aldrich	Cat#HPA042403; RRID:AB_2677980
Mouse monoclonal anti-COUP-TF2	Perseus Proteomics	Cat#PP-H7147-00; RRID:AB_2314222
Mouse monoclonal anti-CGβ	Abcam	Cat#ab9582; RRID:AB_296507
Rat monoclonal anti-PGF	R&D Systems	Cat#MAB2642; RRID:AB_10718412
Rabbit polyclonal anti-TBX3	Abcam	Cat#ab99302; RRID:AB_10861059
Mouse monoclonal anti-SDC1	Abcam	Cat#ab181789
Mouse monoclonal anti-HOPX	Santa Cruz	Cat#sc-398703; RRID:AB_2687966
Rabbit polyclonal anti-cytokeratin23	Proteintech	Cat#24049-1-AP; RRID:AB_2879416
Rat monoclonal anti-ECAD	TAKARA	Cat#M108; RRID:AB_2895157
Mouse monoclonal anti-HLA-ABC	BioLegend	Cat#311402; RRID:AB_314871
Mouse monoclonal anti-HLA-ABC(PE)	BioLegend	Cat#311406; RRID:AB_314875
Mouse monoclonal anti-PD-L1	Cell Signaling Technology	Cat#13684; RRID:AB_2687655
Mouse monoclonal anti-HLA-G	Santa Cruz	Cat#sc-21799; RRID:AB_627938
Rabbit polyclonal anti-ACTIN	Sigma Aldrich	Cat#A5060; RRID:AB_476738
Mouse monoclonal anti-PAX6	BD Biosciences	Cat#561462; RRID:AB_10715442
Goat polyclonal anti-ISL1	R&D Systems	Cat#AF1837; RRID:AB_2126324
Mouse monoclonal anti-MEIS2	Sigma Aldrich	Cat#WH0004212M1; RRID:AB_1842419
Goat polyclonal anti-HAND1	R&D Systems	Cat#AF3168; RRID:AB_2115853
Mouse monoclonal anti-HAND1	Santa Cruz	Cat#sc-390376
Rabbit polyclonal anti-PRTG	Sigma-Aldrich	Cat#HPA032138; RRID:AB_10669675
Rabbit polyclonal anti-DLX5	Sigma-Aldrich	Cat#HPA005670; RRID:AB_1078681
Rabbit polyclonal anti-GABRP	Abcam	Cat#ab26055; RRID:AB_470785
Rabbit monoclonal anti-B7H4	Abcam	Cat#ab252438
Mouse monoclonal anti-B7H4 (PE)	Thermo Fisher	Cat#12-5949-42; RRID:AB_1944340
Mouse monoclonal anti-CD138(FITC)	Miltenyi Biotec	Cat#130-119-927; RRID:AB_2751925
Chemicals, peptides, and recombinant proteins		
DMEM/F12	Sigma-Aldrich	Cat#D6421
Knockout Serum Replacement	Gibco	Cat#10828-028
MEM-NEAA(100x)	Gibco	Cat#11140-050
2-mercaptoethanol	Nakalai Tesque	Cat#21438-82
L-glutamine	Gibco	Cat#25030081
Basic FGF	WAKO	Cat#064-04543
BMP4	R&D Systems	Cat#314-BP
NOGGIN	R&D Systems	Cat#6057-NG
A83-01	WAKO	Cat#039-24111

(*Continued on next page*)

Continued

REAGENT or RESOURCE	SOURCE	IDENTIFIER
PD173074	WAKO	Cat#160-26831
LDN-193188	STEMGENT	Cat#04-0074
Y-27632 dihydrochloride	Tocris	Cat#1254
Recombinant Cas9	Clontech	Cat#632641
Matrigel	Corning	Cat#356230
DRAQ7	Cell Signaling Technology	Cat#7406
Hoechst 33342	WAKO	Cat#346-07951
Alexa-flour palloidin	Invitrogen	Cat#A12379
Critical commercial assays		
Human BMP4 ELIZA Kit	Abcam	Cat#ab231930
Human CGβ ELIZA Kit	Abcam	Cat#ab108638
Human GDF15 ELISA Kit	Proteintech	Cat#KE00108
Guide-it Long ssDNA Production System	Clontech	Cat#632644
Guide-it sgRNA In Vitro Transcription System	Clontech	Cat#632635
Nano-Glo Dual-Luciferase Reporter Assay System	Promega	Cat#N1610
Chromium Single Cell 3′ Library & Gel Beads Kit v3.1	10x Genomics	Cat#PN-120267
NextSeq500/550 High Output v2.5 Kit	Illumina	Cat#20024907
NovaSeq 600 SP Reagent Kit v1.5	Illumina	Cat#20028401
Deposited data		
RNA-seq data	This paper	GEO:GSE175977
Single cell RNA-seq data	This paper	GEO:GSE196365
RNA-seq data of human ESC-derived three germ layers	Cliff et al. (2017)	GEO:GSE101655
RNA-seq data from ESC-derived amnion-like cells	Shao et al. (2017a, 2017b)	GEO:GSE89479
Single cell RNA-seq data from ESC-derived embryonic sac	Zheng et al. (2019)	GEO:GSE134571
Single cell RNA-seq data from cultured human blastocyst	Xiang et al. (2020)	GEO:GSE136447
Single cell RNA-seq data from gastrulation stage huma embryo	Tyser et al. (2021)	http://human-gastrula.net/
Experimental models: Cell lines		
Human embryonic stem cell line KhES-1	Suemori et al. (2006)	N/A
Human embryonic stem cell line KthES-11	Kawase et al. (2021)	N/A
Human induced pluripotent stem cell line 253G1	Nakagawa et al. (2008)	N/A
Mouse embryonic fibroblasts	Oriental Yeast	KBL9284400
DR4 MEF feeder cells	Applied Stem Cell	ASF-1001
Oligonucleotides		
Primers for RT-qPCR, see Table S1	This paper	Table S1
sgRNA target sequence, see STAR Methods	This paper	STAR Methods
Recombinant DNA		
pCAG-hyPBase	Yusa et al. (2011)	N/A
PB-CAG-IRES-Neo^{R}	Ohgushi et al. (2015)	N/A
PL552	Addgene	Cat#68407
pNL3.2[Nluc_minP]	Promega	Cat#E1752

(*Continued on next page*)

Continued

REAGENT or RESOURCE	SOURCE	IDENTIFIER
pGL3.2-8xBMP-RE	This study	N/A
Software and algorithms		
STAR v2.6.1d	Dobin et al. (2013)	https://github.com/alexdobin/STAR
RSEM v1.3.3	Li and Deway (2011)	https://deweylab.github.io/RSEM/
R v4.0.3	The R foundation	https://www.r-project.org
edgeR v3.32.0	Robinson et al. (2010)	https://bioconductor.org/packages/release/bioc/html/edgeR.html
clusterProfiler v3.18.0	Yu et al. (2012)	https://bioconductor.org/packages/release/bioc/html/clusterProfiler.html
TissueEnrich v1.10.1	Jain and Tuteja (2019)	https://www.bioconductor.org/packages/release/bioc/html/TissueEnrich.html
Cell Ranger v4.0.0	10X Genomics	https://github.com/10XGenomics/cellranger
Seurat v4.0.5	Hao et al. (2021)	https://github.com/satijalab/seurat
Seurat Wrapper v0.3.0	N/A	https://github.com/satijalab/seurat-wrappers
Monocle3 v0.2.3.0	Cao et al. (2019)	https://github.com/cole-trapnell-lab/monocle-release
SCENIC v1.2.4	Aibar et al. (2017)	https://github.com/aertslab/SCENIC
GENIE3 v1.12.0	Huynh-Thu et al. (2010)	https://bioconductor.org/packages/3.12/bioc/html/GENIE3.html
RcisTarget 1.10.0	Aibar et al. (2017); Aibar et al. (2016a). 2016b	https://bioconductor.org/packages/3.12/bioc/html/RcisTarget.html
AUcell v1.12.0	Aibar et al. (2017); Aibar et al. (2016a). 2016b	https://bioconductor.org/packages/3.12/bioc/html/AUCell.html
gglopt2 v3.3.3	N/A	https://ggplot2.tidyverse.org/
Heatmaply v1.1.1	Galili et al. (2018)	https://talgalili.github.io/heatmaply/index.html
Corrplot v0.90	Taiyun and Villiam (2021)	https://github.com/taiyun/corrplot
FlowJo v10.7.1	FlowJo	https://www.flowjo.com/
MetaMorph v7.7.3.0	Molecular Devices	N/A
Fiji (ImageJ) v2.1.0/1.53c	NIH	https://fiji.sc/

RESOURCE AVAILABILITY

Lead contact

Further information and requests for the resources and reagents should be directed to and will be fulfilled by the lead contact, Masatoshi Ohgushi (mohgushi@infront.kyoto-u.ac.jp).

Materials Availability

All reagents developed in this study are available from the lead contact with reasonable compensation by the requestor for its processing and shipping.

Data and code availability

RNA sequencing data reported in this paper are available in NCBI Gene Expression Omnibus. This paper also analyses existing publicly available datasets. Accession numbers are listed in the Key resources table.

This paper does not report original codes.

Any additional information required to reanalyze the data reported in this paper is available from the lead contact upon request.

EXPERIMENTAL MODEL AND SUBJECT DETAILS

Pluripotent stem cells

All experiments using the human primed ESC lines KhES-1 and KthES-11 (Kyoto University; Suemori et al., 2006; Kawase et al., 2021) were performed following the human ESC guidelines of the Japanese government. The 253G1 human iPSCs were a gift from S. Yamanaka (Kyoto University; Nakagawa et al., 2008). The KhES-1 cells were mainly analyzed in this study, but the other cell lines were

also tested for some key experiments. Undifferentiated human ESCs/iPSCs were maintained as previously described (Ohgushi et al., 2010, 2015). Cells were cultured on feeder layers of mouse embryonic fibroblasts (MEF; Kitayama Labes; inactivated with 10 μg/mL mitomycin C and seeded at 4 × 10^5 per 6 cm dish) in DMEM/F12/KSR medium (D-MEM/F12 (Sigma) supplemented with 20% KSR additive, 2 mM glutamine, 0.1 mM non-essential amino acids (Invitrogen) and 0.1 mM 2-mercaptoethanol). Recombinant human basic FGF (5 ng/mL, Wako) was added soon after seeding. For cell passaging, ESC colonies were detached by treating them with CTK dissociation solution at 37°C for 5-7 min, tapping the cultures, and then flushing them with a pipette, and recovering *en bloc* from the feeder layer. The detached ESC clumps were broken into smaller pieces by gently pipetting several times, and then these small clumps were transferred onto a MEF-seeded dish. For feeder-free cultures, contaminating MEF cells were removed by incubating the suspension on a gelatin-coated plate at 37°C for 2 h in the maintenance culture medium. In this procedure, MEF cells adhere to the dish's bottom, but ESC clumps do not. The MEF-free ESC clumps were suspended in a MEF-conditioned medium and seeded onto a Matrigel substrate (BD Biosciences). The culture medium containing bFGF was refreshed daily until the next passage.

METHOD DETAILS

Plasmids and transfection procedure

To construct a reporter plasmid for BMP-dependent transcription (pNL3.2-8×BMP-RE), double-stranded oligonucleotides containing eight BMP-responsive elements (AGATCCTCTGGTCACAGGATAATAATCCTGACGCCAGAAAGTCTGGAGGTC) in tandem were synthesized (GeneArt, Invitrogen) and introduced into the pNL3.2[Nluc_minP] vector (Promega). KhES-1 cells stably expressing fluorescence proteins were generated using a Piggybac (PB) transposon system, as described previously (Ohgushi et al., 2015). cDNAs for venus-tagged H2B, eCFP-tagged H2B and mCherry were subcloned into the PB transposon vectors containing a CAG-promoter-driven expression cassette, followed by an IRES-NeoR (a gift from Dr. Niwa). These PB vectors were co-transfected with a *pCAG-hyPBase* expression vector (a gift from Dr. Yusa) using the Lipofectamine Stem reagent (Invitrogen). A few days after the transfection, cells were passaged to the DR4 MEF (Cell Systems)-coated dishes and, on the following day, the medium was switched to a 100 μg/mL G418-containing one to obtain polyclonal stable pools with G418-resistance. Cells expressing fluorescence proteins were collected using a FACS Aria III flow cytometer (BD Biosciences), and used for downstream experiments.

Generation of GATA3 reporter cell line

The gene-targeting strategy for G3KI ESC lines is illustrated in Figure S1A. The guide RNA was designed to target an immediate downstream of the stop codon of the human GATA3 gene (GGCCCTGTGAGCATCGAGCA) and generated using the Guide-it sgRNA In Vitro Transcription System (Clontech). To create a donor template, homology arms to the integration site of the GATA3 gene, the 5′ arm (772bp) and 3′ arm (648 bp), were amplified by PCR using the genome extracted from KhES-1 cells as a template. To eliminate the gRNA target in the 3′ arm of the donor, the PAM sequence was disrupted by PCR-mediated mutagenesis. The 5′ arm was linked with a cDNA for encoding P2A peptide-fused tandem tomato fluorescent proteins in flame. These fragments were integrated into a PL552 vector (Addgene, #68407) that contained a floxed expression cassette of puromycin-resistant genes downstream of the pgk promoter and sequenced. Using this vector as a template, a single-stranded donor for homologous recombination was generated using the Guide-it Long ssDNA Production System (Clontech). The gRNA, single-stranded donor, and recombinant Cas9 proteins (Clontech) were introduced together into the KhES-1 cells by electroporation (Neon device, Invitrogen). Recombinant ESCs were selected with 1 μg/mL puromycin, and the clones harboring both recombined and intact alleles were identified by genomic PCR and sequencing. The resultant clones were transfected with a Cre recombinase expressing vector, and subclones in which a pgk-PuroR cassette was removed were subjected to experiments.

GATA3$^+$ ExE differentiation

For GATA3$^+$ ExE differentiation, human ESCs were collected as clumps, suspended in MEF-conditioned medium, and transferred onto Matrigel-coated dishes. The next day, the culture medium was replaced with fresh media containing A83-01 (1 μM) and PD173074 (0.1 μM), and the medium was refreshed daily. Unless otherwise indicated, fresh DMEM/F12/KSR without bFGF was used as the basal medium. We also tested other media such as MEF-conditioned DMEM/F12/KSR, mTeSR1(Stem Cell Technologies), StemFit AK-03N (AJINOMOTO), CDM (IMDM + Ham's F-12 at 1:1 (Sigma), chemically defined lipid concentrate (Sigma), monothioglycerol (450 μM), 1% ITS-X supplement (WAKO) and purified BSA (3%, WAKO)) and N2B27 (DMEM/F12/GlutaMax + Neurobasal at 1 : 1 (Sigma), 1 × B27 (Gibco), 1 × N2 (Gibco) and 0.1 mM 2-mercaptoethanol) on the different substrates-coated plates (MEF-feeder cells, Matrigel and Laminin-E8 (Nippi)).

Immunostaining

Immunostaining was performed as described previously (Ohgushi et al., 2015). The cells were fixed with 4% PFA at 4°C for 20 min and then permeabilized with 0.1–0.3% Triton X-100 solution. For HLA-ABC, GABRP and PRTG staining, cells were not permeabilized. After incubation in blocking solution such as 2% skim milk, 1% BSA or 10-20% normal donkey serum (Abcam), cells were incubated in the blocking solution containing specific antibodies. The staining was visualized using secondary antibodies conjugated with Alexa Fluor 488, -546, or −647 (Invitrogen). For F-actin staining, Alexa Fluor-conjugated phalloidin (Invitrogen) was used. The nucleus

was stained with DAPI or Hoechst-33342 (WAKO). Experiments were performed at least three times. Images were obtained using a fluorescence microscopy (LASX system, Zeiss) or an inverted microscope (IX81-ZDC, Olympus). For confocal observations, serial images were collected using a CSU-W1 unit (Yokogawa) configured with an IX81-ZDC microscope. Image processing was performed using the MetaMorph and FIJI software.

Western blot analyses

Cells were washed with PBS and treated on the plate with HEPES lysis buffer (50 mM HEPES pH 7.4, 150 mM NaCl, 1 mM EDTA, 1% NP-40, and protease inhibitor cocktail) for 10 min at 4°C with gentle shaking, and total cell extracts were harvested by pipetting. Immediately after adding the appropriate amount of 4 × LDS sample buffer (Invitrogen) to the extracts, the cells were subjected to a brief sonication for complete lysis. After boiling, cell lysates were analyzed by SDS-PAGE and western blotting. A 5% skim milk solution was routinely used as a blocking reagent. In particular, for the detection of phosphorylated proteins, a 2% BSA solution was used for blocking. Images were obtained with an Amersham Imager 600 (Fuji Film) and processed using the FIJI software.

Flow cytometry analyses

To quantify fluorescence protein-expressing cells, cells were dissociated into single cells by TlypLE select and suspended in PBS containing the DNA dye DRAQ-7 (Cell Signaling). The cell suspensions were passed through a mesh filter with 30 μm pores before flow cytometric analyses. Using FACS Aria IIIu flowcytomer, the DRAQ-7-positive population was eliminated as dead cells, and the fluorescence in these individual cells was measured. For the detection of surface protein expression in live cells, dissociated cells were suspended in a culture medium and stood in suspension for 30 min in a CO_2 incubator. The cells were washed with FACS buffer (PBS containing 2% fetal bovine serum) and incubated for 30 min in FACS buffer containing primary antibodies. When needed, staining with fluorescence-labeled secondary antibodies was performed. After washing and suspending in FACS buffer containing DRAQ-7, the cells were subjected to flow cytometry analyses. For HAND1 staining, dissociated cells were fixed with chilled methanol for 10 min. The fixed cells were incubated in blocking solution (10% normal donkey serum) for 30 min, and then incubated in the blocking solution containing primary antibodies for 1 h (or overnight). The cells were stained using secondary antibodies conjugated with AlexaFluor-488 (Invitrogen), and subjected to flow cytometry analyses.

Luciferase reporter assays

The BMP reporter plasmid (pNL3.2-8×BMP-RE) was transfected into ESCs together with the pGL3.2 plasmid for normalization. Cell extracts were prepared using Passive Lysis Buffer (Promega), and luciferase reaction was induced using the Nano-Glo Dual-Luciferase Reporter Assay System (Promega). Luciferase activity of firefly and Nano-Luc was evaluated as luminescence measured using a SpectraMax iD3 plate reader (Molecular Devices). Luciferase activity units were represented as the ratio of Nano-Luc to firefly luminescence.

Quantitative real-time PCR

Total RNA was extracted using the RNAeasy Mini Kit (Qiagen), and cDNA was synthesized using SuperScript II reverse transcriptase (Invitrogen). The PCR reaction mixture was prepared on a 96-well plate using a Power SYBR Green PCR Master Mix according to the manufacturer's instructions (Applied Biosystems). The primer sets are listed in Table S1. They were run in triplicate on a 7500 Fast Real-Time PCR System (Applied Biosystems). The expression level of each mRNA was estimated according to the corresponding standard curve and normalized to that of GAPDH. Data are displayed as percentages to a maximum value or relatives to a control sample.

Live imaging

Live imaging was performed as previously described (Ohgushi et al., 2010) using an inverted microscope (IX81-ZDC, Olympus) that was equipped with a stepper filter wheel (Ludl) and a cooled EM-CCD camera (ImagEM, Hamamatsu Photonics)-. For a confocal observation to monitor syncytium formation and cell division history, a single slice of the image was recorded using a CSU-W1 unit (Yokogawa) configured with an IX81-ZDC microscope.

Capture of syncytia formation

Two lines of KhES-1 cells expressing H2B-venus or mCherry were treated with AP for 4 days on the different culture plates. On day 4, these cultures were dissociated and mixed at 1 : 1 ratio. The mixed cells were seeded on Matrigel-coated 6-well plates (2.5×10^5 cells per well) and further cultured in the DMEM/F12-based medium (D-MEM/F12 supplemented with 4% KSR additive, 1% ITS-X (Gibco), 0.3% BSA (Invitrogen), and 0.1 mM 2-mercaptoethanol and 2.5 μM Y-27632). For live imaging, the mixed cells were seeded on Matrigel-coated 35 mm dishes (Idibi) and time-lapse recording was started on the next day. After 6 days of mixing, the cells were dissociated and harvested for flow cytometric analyses. To validate protein expression in syncytial cells, dissociated cells were suspended in a culture medium and stood in suspension for 1 h in a CO_2 incubator. Double-positive cells (2×10^5 cells) were collected using a FACS Aria IIIu. Western blot analyses were done as described above. For the comparison, undifferentiated ESCs (non-labeled) were subjected to a similar procedure.

Bulk-RNA sequence and data analyses

Total RNA was harvested as described above. Sequencing libraries were prepared from 1 μg total RNA using the TruSeq Standard mRNA LT Sample Preparation Kit (Illumina) and sequenced by Illumina NextSeq500 (Illumina) using NextSeq500/550 High Output v2.5 Kit (Illumina) to obtain single-end 75 nt reads. Fastq files were generated using BaseSpace Onsite (Illumina). They were deposited to the Gene Expression Omnibus (GEO) database (GSE175977).

Sequence reads were aligned against GRCh38 genome assembly using STAR (version 2.6.1d, Dobin et al., 2013). Read counts and transcripts per million (TPM) values of each gene were quantified and calculated using RSEM (version 1.3.3, Li and Deway, 2011). All TPM values used in this study were provided in Table S2. The read counts and TPM values of each sample were imported into the R platform (version 4.0.3) as the matrix data. The genes for which the sum of read counts of all given samples was <10 were excluded as ultra-low expressed genes for the following analyses. The read count matrix was provided to the R package edgeR (version 3.32.0, Robinson et al., 2010), and differential gene expression between the two samples was assessed using an exact test. The DEGs were defined as genes that were expressed with a p-value < 0.01 and a false discovery rate <0.05. For gene ontology and tissue enrichment analyses, upregulated genes (log2[fold change] > 4) were extracted from DEGs and provided as input to the R package clusterProfiler (version 3.18.0, Yu et al., 2012) and TissueEnrich (version 1.10.1, Jain and Tuteja, 2019), respectively. TPM was used as a measure of relative transcript abundance. Hierarchical clustering was performed with the R function *as.dist* and *hclust* using 'ward.D2' based, and principal component analyses were performed using the *prcomp.*

Single-cell RNA sequence and data analyses

For library preparation and sequencing

The AP-treated G3KI#2-5 ESCs were dissociated by TrypLE select into single cells and suspended in PBS containing DRAQ-7. After the cell suspension were passed through a mesh filter with 30 μm pores, DRAQ-7-negative live cells were isolated as single cells using a Flow cytometer. This preprocessing for reducing the incorporation of debris, large clumps or dead cells in the loading samples is crucial to minimize the risk for microfluidic chip clogs in the following step. The sorted cells were suspended in 0.04% BSA-containing PBS, diluted into an optimal concentration, and then they were applied to a chromium controller (10x Genomics). A Chromium Single Cell 3′ Library & Gel Beads Kit v3.1 (10x Genomics) was used to generate oligo-dT-primed cDNA libraries following the manufacturer's protocol. The cDNA library for each sample was separately prepared and sequenced on an Illumina NovaSeq 6000 (Illumina) using the NovaSeq 6000 SP Reagent Kit v1.5 (Illumina). Sequence reads were aligned against GRCh38 genome assembly using the cellranger count command of Cell Ranger (version 4.0.0) to generate a count matrix of unique molecular identifiers for each gene per cell. They were deposited to the GEO database (GSE196365).

Data processing for analyses on a single dataset

Data processing was done on the R platform using the Seurat package (version 4.0.5, Hao et al., 2021). The Seurat object was generated using genes expressed in at least ten cells and cells including at least ten genes. For quality control, cells that expressed <4,000 genes, and >15% of mitochondrial genes were filtered out. A standard data processing workflow including normalization, finding highly variable genes and scaling were done using default parameters. The cell cycle effect was assessed using the *CellCycleScoring* function and was regressed by *vars.to.regress* option implemented in the *ScaleData* function. To reduce the dimensionality of the datasets, the *RunPCA* function was conducted using the top 2,000 highly variable genes. After nonlinear dimensional reduction was conducted with the *RunUMAP* function, cells were projected into a two-dimensional space using UMAP. We tested different numbers of PCs and selected the appropriate PCs for the *RunUMAP* function. Cell clusters of the day 4 dataset were identified using the *FindClusters* function by the first 15 PCs with the resolution parameter set to 0.5. Signature scores for each cell were computed using the *AddModuleScore* function using the given genelist. To identify DEGs among the clusters of interest, we used the *FindMarkers* function. Statistical significance was tested using a Wilcoxon rank sum test, and genes with adjusted p values less than 0.01 were considered significant.

Processing of time-series datasets as a single object

To revolve temporal dynamics of cell state transition, three Seurat objects were generated independently, and then they were integrated into a single object simply using the *merge* function. After omitting low-quality cells, an integrated object contained total 5,123 cells (1,469 cells from day 2, 1,773 cells from day 3 and 1,890 cells from day 4 samples). Using this object, normalization, finding highly variable genes and scaling were done as described above. Nonlinear dimensional reduction was conducted with the *RunUMAP* function using the first 65 PCs, and all cells were projected into a two-dimensional space using UMAP. For the trajectory inference and pseudotime analyses, we used the R packaged Monocle3 (version 0.2.3.0, Cao et al., 2019). The processed Seurat object was imported as a Monocle object using the *as.cell_data_set* function implemented in the SeuratWrappers package (version 0.3.0). We identified cell clusters and partitions using the *cluster_cells* function with the *resolution* set to 0.001, and then fitted a principal graph using the *learn_graph* function. For pseudotime estimation, we defined the beginning root of the trajectory using the *order_cells* function considering the *GATA3* and *POU5F1* expression levels. Each cell was colored by the pseudotime and plotted on a UMAP space using the *plot_cells* function. According to the estimated trajectory, cells were divided into one outlier and three groups (ExE-A, -B or -C), and extracted using the *choose_graph_segments* function. We subtracted the outlier cells from the original integrated Seurat object and rebuilt a new one using the remaining cells. Annotation information including cell populations and computed pseudotimes were imported into a metadata slot of the object. The new Seurat object consisted of 5,039 cells (1,867 cells of ExE-A, 2,839 cells of ExE-B and 333 cells of ExE-C). Using this rebuilt object, normalization, finding highly variable genes, scaling, nonlinear dimensional reduction and UMAP projection were done again as described above.

Processing for the comparison with publish single cell transcriptome

To evaluate AP-treated cells with the amnion-sac model, single-cell data for 'Posteriorized embryonic-like sacs' and 'mixture of amniotic ectoderm-like cells (transwell) and H9 cells' were obtained from GEO (accession number GSE134571) (Zheng et al., 2019). Sequence reads of the AP-treated cells (day 2) and the amnion-sac were aligned against the same reference genome assembly. For quality control of the AP-treated cells, cells that expressed <4,000 genes, and >15% of mitochondrial genes were filtered out, and used as a query data. For the reference, two downloaded datasets were integrated into a single Seurat object using the *merge* function. For quality control, cells that expressed <3000 genes and >8% of mitochondrial genes were filtered out to generate a reference object consisting of 11,212 amnion-sac cells. Normalization, finding highly variable genes, scaling and dimensional reduction were done as described, and the reference UMAP model was computed using the *RunUMAP* function with the 'return.model' set to 'TRUE'. After normalization and finding highly variable genes were done following the standard workflow, we projected the query data onto the reference UMAP using the *FindTransferAnchors* and *MapQuery* functions. To plot all cells in the same UMAP space, we applied 'de novo visualization' (Hao et al., 2021). The reference and projected query dataset were merged, and then new UMAP was computed by the *RunUMAP* function using pca and ref.pca as dimensional reductions for the inputs.

The expression data for single cells of human peri-implantation embryos and the cell annotation information were downloaded from Gene Expression Omnibus (GEO) with accession number GEO136447 (Xiang et al., 2020). The data for cells of the gastrulating human embryo were downloaded from the authors' website (http://human-gastrula.net/), including the read count matrix and cell annotation data (Tyser et al., 2021). Data of these public datasets and the single-cell data generated in this study were preprocessed using the R as follows. First, we defined the intersect of gene names shared by all datasets. For a subset of genes, the Xiang et al. count matrix included alternative transcripts. To make this dataset compatible with the gene names of the others, for genes with multiple transcripts we retained the transcript which was detected in the largest number of cells. This resulted in a merged read count matrix for 22,691 shared genes in 21,410 cells in total. A single Seurat object was generated from the merged matrix and analyzed. Genes that were detected (read count >0) in less than 3 cells were filtered out. We inspected the data produced by each study and retained only cells that satisfied the following conditions:

- for our in-house data: 3000 < detected genes <8000, 3% < mitochondrial reads <12%.
- for the Xiang et al. data: detected genes >7000, mitochondrial reads <12%.
- for the Tyser et al. data: mitochondrial reads <3%, and total read count >100,000.

In addition, cells annotated as ''Hemogenic Endothelial Progenitors'' and ''Erythroblasts'' in the Tyser dataset were omitted. We noticed that cells annotated as ''ICM'' in Xiang dataset highly expressed several trophoblast markers including GATA3, making their reliability as a reference for cell-type classification ambiguous. Therefore, we also omitted these cells in our analyses. For conveniences, cells annotated as ''Emergent Mesoderm'', ''Advanced Mesoderm'' and ''Nascent Mesoderm'' were re-annotated together as ''Mesoderm''. Cells annotated as ''Non-Neural Ectoderm'' were re-annotated in our analyses as ''Ectoderm (amniotic/embryonic)'', a term used in their published paper (Tyser et al., 2021). These processing resulted in a Seurat object consisting of 22,679 genes and 6,590 cells. We first tried to construct a reference object by merging Xiang and Tyser dataset, but this revealed that cells were almost perfectly separated by the studies. We therefore integrated these two datasets using functions of the Seurat package as follows. Data for of each study was normalized and 2,000 highly variable genes were detected. Shared variable features were picked up using the *SelectIntegrationFeatures* function. Subsequently, the data was integrated using the *FindIntegrationAnchors* and *IntegrateData* functions. After integration, the combined data was scaled, and dimensionality reduction was performed using PCA and UMAP based on the first 30 PCs. Visual inspection revealed that batch effects had been removed successfully, and we used this integrated data as a reference. As query data, the processed Seurat object of AP-treated cells (day 2 to day 4) was used. Projecting the query data onto the reference UMAP and ''de novo visualization'' were done as described above.

SCENIC- analyses

Gene regulatory networks were inferred using R package SCENIC (v.1.2.4) (Aibar et al., 2016a, 2016b, 2017). Before SCENIC analyses, omitting low-quality cells, normalizing and cell clustering was done by a Seurat package as describe before. The log-normalized count matrix was extracted from the processed Seurat object together with the cell annotation data. This matrix was prefiltered using the *geneFiltering* function in default settings. Using the filtered matrix as an input, potential transcription factor targets were inferred by running GENIE3 (v1.12.0, Huynh-Thu et al., 2010). Building co-expression modules, inferring potential regulons and scoring regulon activities in each cell were done by running three SCENIC functions, *runSCENIC_1_coexNetwork2modules*, *runSCENIC_2_creatRegulons* and *runSCENIC_3_scoreCells*, respectively. The results provided a matrix of AUCell values that represent the activity of each regulon in each cell. The AUCell values of specific regulons were imported into the Seurat object as a metadata slot and used for visualization of regulon activities in the UMAP space.

External data

Gene lists for EPI, PrE and TrB (Figure 1N), pre-CTB, post-CTB, early-STB, STB, early-EVT, and EVT (Figures 2B, 2C, S2C, and S2D) were obtained from the report of Xiang et al. (see Tables S1 and S4 in Xiang et al., 2020). Gene lists for calculating STB signature score were generated by combing together genes annotated as early-STB- and STB-enriched ones (Figure 6F). Transcriptional information

on the human amniotic ectoderm is still limited. Therefore, we applied the single-cell data of post-implantation stage of cynomolgus monkey (Ma et al., 2019). For constructing a gene list to calculate signature score for the amnion, we extracted the genes annotated as 'E-AM' or 'L-AM' in the column of 'cluster' (see Table S6 in Ma et al., 2019). Gene symbols were converted to the human version using an annotation table downloaded from Ensembl. This gene list included several typical trophoblast genes. Genes showing high expression in the human placenta were selected by extracting the genes annotated as 'Placenta' in the column of 'max_organ' (Cao et al., 2020, their Table S2), and an amnion-unique gene list were generated by subtracting the placenta genes from the amnion gene list.

Other datasets used in this study were downloaded from GEO with accession numbers GSE101655 (Cliff et al., 2017) and GSE89479 (Shao et al., 2017a-).

Graphical presentation

Correlation heatmaps and gene expression heatmaps were generated using the R package corrplot (version 0.84, Taiyun and Viliam, 2021) and heatmaply (version 1.1.1, Galili et al., 2018), respectively. Graphic visualization of single-cell transcriptome data was done using *DimPlot*, *FeaturePlot*, *VlnPlot*, *DotPlot* and *DoHeatmap* functions implemented in Seurat with some modifications using the R package ggplot2 (version 3.3.3). Flow cytometric data were visualized using the FlowJo software (version 10.7.1). All other graphs were generated using ggplot2.

QUANTIFICATION AND STATISTICAL ANALYSIS

Quantification methods are described in individual figure legends or in STAR Methods. Results are indicated as the means. Error bars represent standard deviations and n in the legends is the number of experiments. Statistical significance (two-sided) was tested by Student's t-test, Wilch t-test or Wilcoxon signed-rank test for two-group comparison, Tukey's (among all groups), or Dunnett's test (versus control) for multiple-group comparison using R.